Ribonuclease inhibitor 1 regulates erythropoiesis by controlling GATA1 translation

Vijaykumar Chennupati,[1] Diogo F.T. Veiga,[2] Kendle M. Maslowski,[3] Nicola Andina,[4,5] Aubry Tardivel,[3,4,5] Eric Chi-Wang Yu,[3] Martina Stilinovic,[4,5,6] Cedric Simillion,[5,7] Michel A. Duchosal,[8] Manfredo Quadroni,[9] Irene Roberts,[10] Vijay G. Sankaran,[11,12] H. Robson MacDonald,[1] Nicolas Fasel,[3] Anne Angelillo-Scherrer,[4,5] Pascal Schneider,[3] Trang Hoang,[2] and Ramanjaneyulu Allam[4,5]

[1]Ludwig Center for Cancer Research, University of Lausanne, Lausanne, Switzerland. [2]Institute of Research in Immunology and Cancer, University of Montreal, Montreal, Quebec, Canada. [3]Department of Biochemistry, University of Lausanne, Lausanne, Switzerland. [4]Department of Hematology, Inselspital, Bern University Hospital, [5]Department of BioMedical Research, [6]Graduate School of Biomedical Science, and [7]Interfaculty Bioinformatics Unit, University of Bern, Bern, Switzerland. [8]Service and Central Laboratory of Hematology, Centre Hospitalier Universitaire Vaudois (CHUV), University Hospital of Lausanne, Lausanne, Switzerland. [9]Protein Analysis Facility, University of Lausanne, Lausanne, Switzerland. [10]Department of Paediatrics and MRC Molecular Haematology Unit, Oxford University; Weatherall Institute of Molecular Medicine, John Radcliffe Hospital, Oxford, United Kingdom. [11]Division of Hematology/Oncology, Boston Children's Hospital, and Department of Pediatric Oncology, Dana-Farber Cancer Institute, Harvard Medical School, Boston, Massachusetts, USA. [12]Broad Institute of MIT and Harvard, Cambridge, Massachusetts, USA.

Ribosomal proteins (RP) regulate specific gene expression by selectively translating subsets of mRNAs. Indeed, in Diamond-Blackfan anemia and 5q$^-$ syndrome, mutations in RP genes lead to a specific defect in erythroid gene translation and cause anemia. Little is known about the molecular mechanisms of selective mRNA translation and involvement of ribosomal-associated factors in this process. Ribonuclease inhibitor 1 (RNH1) is a ubiquitously expressed protein that binds to and inhibits pancreatic-type ribonucleases. Here, we report that RNH1 binds to ribosomes and regulates erythropoiesis by controlling translation of the erythroid transcription factor GATA1. *Rnh1*-deficient mice die between embryonic days E8.5 and E10 due to impaired production of mature erythroid cells from progenitor cells. In *Rnh1*-deficient embryos, mRNA levels of *Gata1* are normal, but GATA1 protein levels are decreased. At the molecular level, we found that RNH1 binds to the 40S subunit of ribosomes and facilitates polysome formation on *Gata1* mRNA to confer transcript-specific translation. Further, RNH1 knockdown in human CD34$^+$ progenitor cells decreased erythroid differentiation without affecting myelopoiesis. Our results reveal an unsuspected role for RNH1 in the control of GATA1 mRNA translation and erythropoiesis.

Introduction

Regulation of gene expression is important for normal development. Recent studies show that ribosomal proteins (RPs) regulate gene expression by selectively facilitating translation of specific mRNAs (1, 2). For example, RPL38 specifically enhances translation of a subset of Hox mRNAs (3). Mutations in RPs impair ribosome function and cause macrocytic anemia in Diamond-Blackfan anemia (DBA), a congenital BM failure syndrome, and in 5q$^-$ syndrome, a subtype of myelodysplastic syndrome (4). Surprisingly, the majority of clinical symptoms are related to erythropoiesis. In support of these observations, ribosomal deficiencies in DBA impair translation of transcripts essential for erythroid differentiation (5, 6). How RPs regulate specific gene expression and how mutations in RPs lead to tissue-specific phenotypes are areas of active investigation.

Ribonuclease inhibitor 1 (RNH1, also known as RI) is a ubiquitously expressed 50 kDa leucine-rich repeat (LRR) protein (7). It is mainly localized in the cytosol, but can also be found in the nucleus and mitochondria (8). RNH1 was the first LRR protein to be crystallized, revealing a horseshoe-shaped 3D structure (9). The human *RNH1* gene evolved via gene duplication and is conserved among mammalian species, with human, porcine, mouse, and rat RNH1 proteins sharing 66% identity (10).

Multiple biological roles have been proposed for RNH1. It binds to and inhibits ribonucleases, such as RNase A, RNase 1, eosinophil-derived neurotoxin (EDN, also known as RNase 2), and RNase 4 (7). RNH1 affinity for ribonucleases is the key determinant factor for RNase cytotoxicity; only ribonucleases that evade RNH1 can kill a cell. RNH1 also binds to angiogenin (ANG), suggesting a possible role in neovascularization (11), but the extent to which RNH1 may regulate angiogenesis remains unclear. Further, RNH1 contains numerous cysteine residues (e.g., 32 in human RNH1), whose sulfhydryl groups might play key structural roles and protect from oxidative damage (7, 12). There are several conflicting reports about the role of *RNH1*. For example, siRNA knockdown of *RNH1* does not sensitize cells to noncytotoxic RNases, and its role in oxidative damage is not firmly established (7, 8, 12, 13). However, despite these observations, the physiological functions of RNH1 remain unexplored.

In this study, we describe an unsuspected role for RNH1 in embryonic erythropoiesis and erythroid differentiation. We find that RNH1 is a ribosomal-associated protein that regulates erythropoiesis by controlling translation of the erythroid transcription factor (TF) GATA1. Like *Gata1*-deficient mice, *Rnh1*-deficient mice die from anemia in utero.

Authorship note: VC, DFTV, KMM, and NA contributed equally to this work. PS and TH contributed equally to this work.
Conflict of interest: The authors have declared that no conflict of interest exists.
Submitted: May 15, 2017; **Accepted:** February 1, 2018.
Reference information: *J Clin Invest*. 2018;128(4):1597–1614.
https://doi.org/10.1172/JCI94956.

Table 1. Genotype table

Genotypes of litters obtained by intercrossing *Rnh1*$^{+/-}$

Stages	Number of pups	+/+	+/–	–/–
E8.5	32	8	13	11[A]
E9.5	78	22	35	21[A]
E10.5	28	5	15	0[B]
E11.5	16	5	11	0
Pups	228	77	151	0

[A]Abnormal compared with WT. [B]All KO embryos were degenerated and residual tissue was found. *Rnh1*-heterozygous (*Rnh1*$^{+/-}$) mice were intercrossed. Genotypes of offspring were determined at different gestational days or after birth, as shown.

Results

Embryonic lethality in Rnh1-deficient mice. To gain insight into the biological function of RNH1, *Rnh1*-deficient (*Rnh1*$^{-/-}$) mice were generated through homologous recombination (Figure 1, A and B). When *Rnh1*-heterozygous (*Rnh1*$^{+/-}$) mice were intercrossed, both *Rnh1*$^{+/+}$ (n = 77) and *Rnh1*$^{+/-}$ (n = 151) mice were observed at the expected 1:2 ratio, but *Rnh1*$^{-/-}$ mice were strikingly absent (Table 1). Similar results were also found in Neo cassette–deleted *Rnh1*$^{-/-}$ mice (data not shown). We next examined embryonic development and found that *Rnh1*$^{-/-}$ embryos developed normally before E7.25 (Supplemental Figure 1A; supplemental material available online with this article; https://doi.org/10.1172/JCI94956DS1), but showed overall growth retardation between E8.5 and E10, with a severe decrease in blood levels in the yolk sac and in the embryo proper (Figure 2, A and B, and Supplemental Figure 1B and Table 1). At this time point, major developmental features, such as chorioallantoic fusion, rotation of the embryo, neural tube closure, and formation of head structures, were present. The complete absence of viable embryos after E10.5 indicated an essential role for *Rnh1* during this developmental window.

Defective embryonic erythropoiesis in Rnh1-deficient mice. Histological examination revealed a profound decrease of erythroid cells in yolk sac blood islands (Figure 2C) and in the placenta (Figure 2D). In addition, the few erythroid cells in yolk sac blood islands of *Rnh1*$^{-/-}$ embryos showed reduced staining with the heme-specific dye benzidine, indicative of a reduced load of hemoglobin (Figure 2E). Endothelium-lined blood vessels were, however, similar in *Rnh1*$^{+/-}$ and *Rnh1*$^{-/-}$ yolk sacs (Figure 2C), and other tissues of mesodermal origin such as somites and myocardium were present (Supplemental Figure 1, C and D). We confirmed that *Rnh1* mRNA was absent in the yolk sac of *Rnh1*$^{-/-}$ embryos (Figure 2F). Since compromised vasculogenesis could affect embryonic erythropoiesis (14), we checked blood-vessel formation in *Rnh1*$^{-/-}$ embryos by immunostaining with Pecam-1 (CD31) and by flow cytometry. Blood-vessel formation was intact in *Rnh1*$^{-/-}$ embryos, as judged by Pecam-1 (CD31) immunostaining (Figure 2H). Similar percentages of CD31$^+$ cells were also detected by flow cytometry in all genotypes, with a moderate increase in *Rnh1*$^{-/-}$ yolk sacs (Figure 2G). Therefore, anemia was not associated with defective vasculogenesis. During development, the endothelial and hematopoietic lineages originate from a common precursor, the hemangioblast (15). The presence of Pecam-1$^+$ endothelial cells in *Rnh1*$^{-/-}$ embryos indicates that hemangioblasts were produced in these embryos and that the defect was hematopoietic specific.

The first wave of hematopoiesis is transient and takes place in the yolk sac, giving rise to a single lineage-restricted population of embryonic-primitive erythroid (EryP) cells (16). In both humans and mice, yolk sac–derived EryP cells support the rapid growth of the embryo during early embryonic development (17). Our observations so far are consistent with the view that embryonic death may be attributed to severely decreased blood cell formation and anemia. Interestingly, the phenotype of *Rnh1*-deficient embryo is similar to those of *Gata1*- and *Gata2*-deficient embryos (18). Nonetheless, mRNA levels of *Gata1* and *Tal1/SCL*, 2 TFs that are essential for embryonic erythropoiesis (19, 20), were not affected (Figure 2I) despite reduced erythroid cells in the *Rnh1*$^{-/-}$ yolk sac (Figure 2C). α-Fetoprotein (*Afp*), the fetal equivalent of serum albumin, was also similarly expressed in *Rnh1*$^{+/+}$ and *Rnh1*$^{-/-}$ yolk sacs (Figure 2I). We also assessed the ability of E8–E9.5 yolk sac–derived cells to form erythroid colonies using a methylcellulose colony-forming assay. In comparison with *Rnh1*$^{+/+}$ and *Rnh1*$^{+/-}$, the number of *Rnh1*$^{-/-}$ colonies was significantly decreased (Figure 2J). Control yolk sac colonies displayed an erythroid burst-forming unit–like (BFU-E–like) morphology and contained erythroid cells. *Rnh1*$^{-/-}$ yolk sac colonies had a similar morphology, but with pale color, and contained less mature erythroid cells (Supplemental Figure 2, A and B). FACS analysis of colony cells revealed that erythroid cells expressing Ter119 and CD71 (also known as transferrin receptor 1) could develop from *Rnh1*-deficient progenitors, but with a markedly decreased frequency compared with *Rnh1*-proficient cells (Supplemental Figure 2C). These data suggest that an intrinsic differentiation defect of progenitor cells precedes the appearance of anemia and the growth defect phenotype. Although the onset of erythropoiesis can occur in *Rnh1*$^{-/-}$ embryos, it is profoundly decreased.

Rnh1 expression during embryonic development. In the adult, *Rnh1* is expressed ubiquitously. However, *Rnh1* expression during embryonic development has not been investigated. *Rnh1* expression increased from E8 to E9.5 (Figure 3A) and, at E9.5, was 7-fold higher in the yolk sac compared with the embryo proper (Figure 3B), coinciding with the site of primitive erythropoiesis (17). It has been reported that RNH1 is highly expressed in erythrocytes (21). We indeed found colocalization of immunostainings for RNH1 and Ter119, a marker of erythroid cells, in the yolk sac and embryo proper of E10.5 WT embryos, in line with a role for RNH1 in embryonic erythropoiesis (Figure 3C and Supplemental Figure 3). High expression of the *Rnh1* gene in Ter119$^+$ erythroid cells during embryonic development concurs with a role for *Rnh1* in embryonic erythropoiesis.

Rnh1 regulates erythroid differentiation. Hematopoietic stem/progenitor cells (HSPCs) that give rise to primitive hematopoiesis are highly enriched in the population of c-Kit$^+$CD41$^+$ cells from the yolk sac (22–24). These cells are transient progenitor populations distinct from later HSC populations that emerge. FACS analysis revealed that the percentage of c-Kit$^+$CD41$^+$ (HSPC) cells present in yolk sacs was comparable in all genotypes (Figure 3D). This observation excludes the possibility that the phenotype of *Rnh1*-deficient embryos may result from defects in HSPC generation. The paucity of nucleated erythroid cells in blood islands of

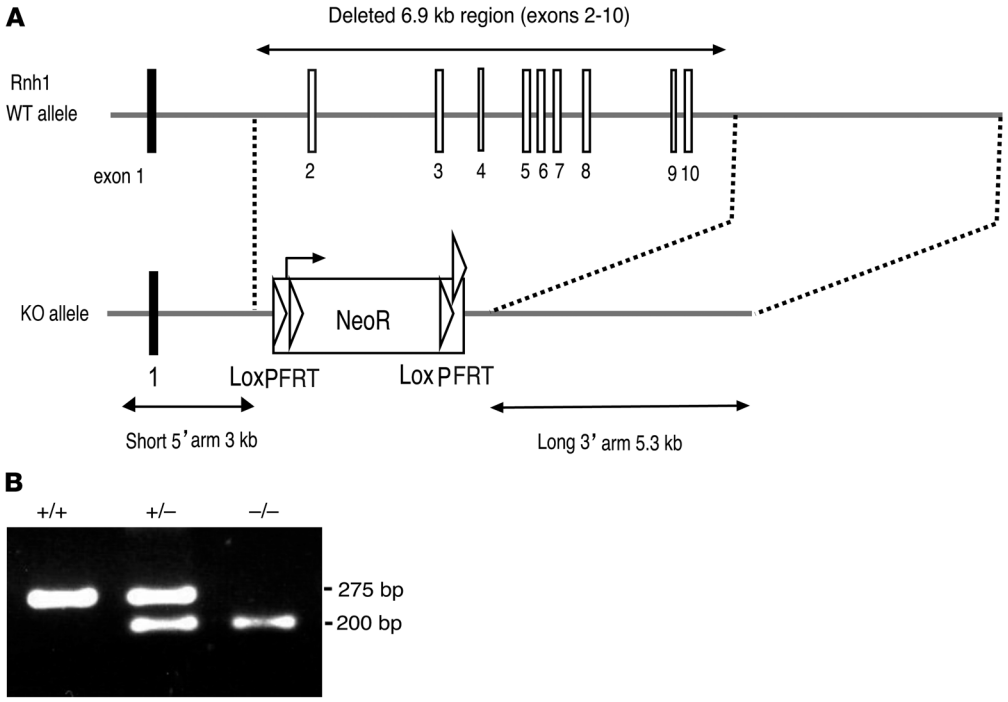

Figure 1. Generation of *Rnh1*$^{-/-}$ mice. (**A**) A 15.1 kb region used to construct the targeting vector was first subcloned from a positively identified C57BL/6 (RP23:210J2) BAC clone using a homologous recombination-based technique. The region was designed such that the long homology arm extended 5.30 kb 3′ to exon 10. The short homology arm is located on the 5′ side of exon 2 and is 2.96 kb long. The Neo cassette replaces 6.89 kb of the gene, including exons 2–10. (**B**) DNA isolated from mouse embryos was genotyped by PCR. Primers were designed to distinguish WT and neo cassette gene sequence. 275 bp size corresponds to WT, and 200 bp size corresponds to knockout mice.

Rnh1-deficient yolk sacs (Figure 2C) led us to analyze E8.5 and E9.5 yolk sac cells by flow cytometry for the erythroid markers Ter119 and CD71. This analysis revealed that EryP cells (Ter119$^+$ and CD71$^+$) were significantly decreased in *Rnh1*-deficient yolk sacs (Figure 3E), while HSPCs were not affected (Figure 3D). We also found more binucleated erythroblast in *Rnh1*$^{-/-}$ yolk sac (Figure 3F), indicating an ineffective erythropoiesis. Together, these data suggest that *Rnh1* is required for efficient differentiation of HSPCs into EryP cells, a process essential for embryonic growth and survival. Since colony assays are based on the capacity of these progenitors to give rise to erythroid cells in vitro, these observations explain why colony numbers are decreased (Figure 2J), but not the actual frequency of HSPCs.

Decreased splenic erythropoiesis in Rnh1$^{+/-}$ *adult mice*. Heterozygous (*Rnh1*$^{+/-}$) mice survived normally and did not show any phenotypic abnormalities, suggesting that 1 allele of *Rnh1* is sufficient for its function. Because our results suggest that Rnh1 regulates erythroid differentiation, we checked to determine whether *Rnh1* haploinsufficiency decreased adult erythropoiesis. While there was no difference in erythroid cell numbers in *Rnh1*$^{+/-}$ BM compared with WT littermates (Figure 4, A and B), erythroid cells in the spleen were significantly decreased (Figure 4, C and D). All 4 erythroid subpopulations, distinguished by differential expression of Ter119 and CD71 (25), were decreased in *Rnh1*$^{+/-}$ spleen compared with *Rnh1*$^{+/+}$ (Figure 4, C and D). Further, FACS forward scatter (indicator of cell size) was also increased in *Rnh1*$^{+/-}$ erythroid cells, indicating decreased erythroblast maturation (25) (Figure 4E). In contrast, there was no difference in numbers of T cells, B cells, and macrophages in the spleen (Figure 4F). Therefore, *Rnh1* is haplo-insufficient for erythropoiesis in the spleen, further pointing to the importance of *Rnh1* in maintaining erythropoiesis.

RNH1 deficiency decreases Gata1 mRNA translation. To get clues on the mechanism(s) causing decreased erythropoiesis in *Rnh1*$^{-/-}$ embryos, we performed a transcriptome analysis on *Rnh1*$^{+/+}$, *Rnh1*$^{+/-}$, and *Rnh1*$^{-/-}$ yolk sacs. There was no change between *Rnh1*$^{+/+}$ and *Rnh1*$^{+/-}$ gene expression patterns, but 628 genes were significantly lower, including genes of mature erythrocytes and genes involved in erythrocyte differentiation, while 273 genes were more expressed in *Rnh1*$^{-/-}$ compared with *Rnh1*$^{+/+}$ (Figure 5A and Supplemental Table 1). A phenotype enrichment analysis revealed hematopoietic defects, such as abnormal blood coagulation, hemostasis, and erythrocyte physiology, as main gene signatures among downregulated genes, in tight agreement with hematopoiesis and erythroid differentiation defects observed in *Rnh1*$^{-/-}$ mice (Supplemental Figure 4A and Supplemental Table 2).

Several TFs are required for erythropoiesis. We applied gene set enrichment analysis (GSEA) in a large data set of ChIP-sequencing (ChIP-seq) studies to determine whether targets of hematopoietic TFs were differentially regulated in the transcriptome of *Rnh1*$^{-/-}$ yolk sacs (see Methods). GSEA scores for most tested regulators, including essential erythropoietic regulators such as GATA1, LDB1, TAL1 and PPARG, were remarkably similar, indicating that their target genes were less expressed in the *Rnh1*$^{-/-}$ yolk sac (Figure 5B and Supplemental Figure 4B and Supplemental Table 3). This global downregulation of hematopoietic TF target genes, but not the TFs themselves, suggests that a posttranscriptional mechanism affects TF gene function, particularly in the erythroid lineage. In support of this hypothesis, a Western blot analysis performed on total *Rnh1*-deficient embryos revealed decreased protein levels of GATA1 (Figure 5C; see complete unedited blots in the supplemental material). We focused on GATA1 because it was top ranked by GSEA analysis and because it is an important hematopoietic TF, without which erythropoiesis does not take place at all developmental stages in mice and humans (26, 27). The GATA1 deficit in *Rnh1*$^{-/-}$ embryos did not entirely result from a reduced number of erythroid cells,

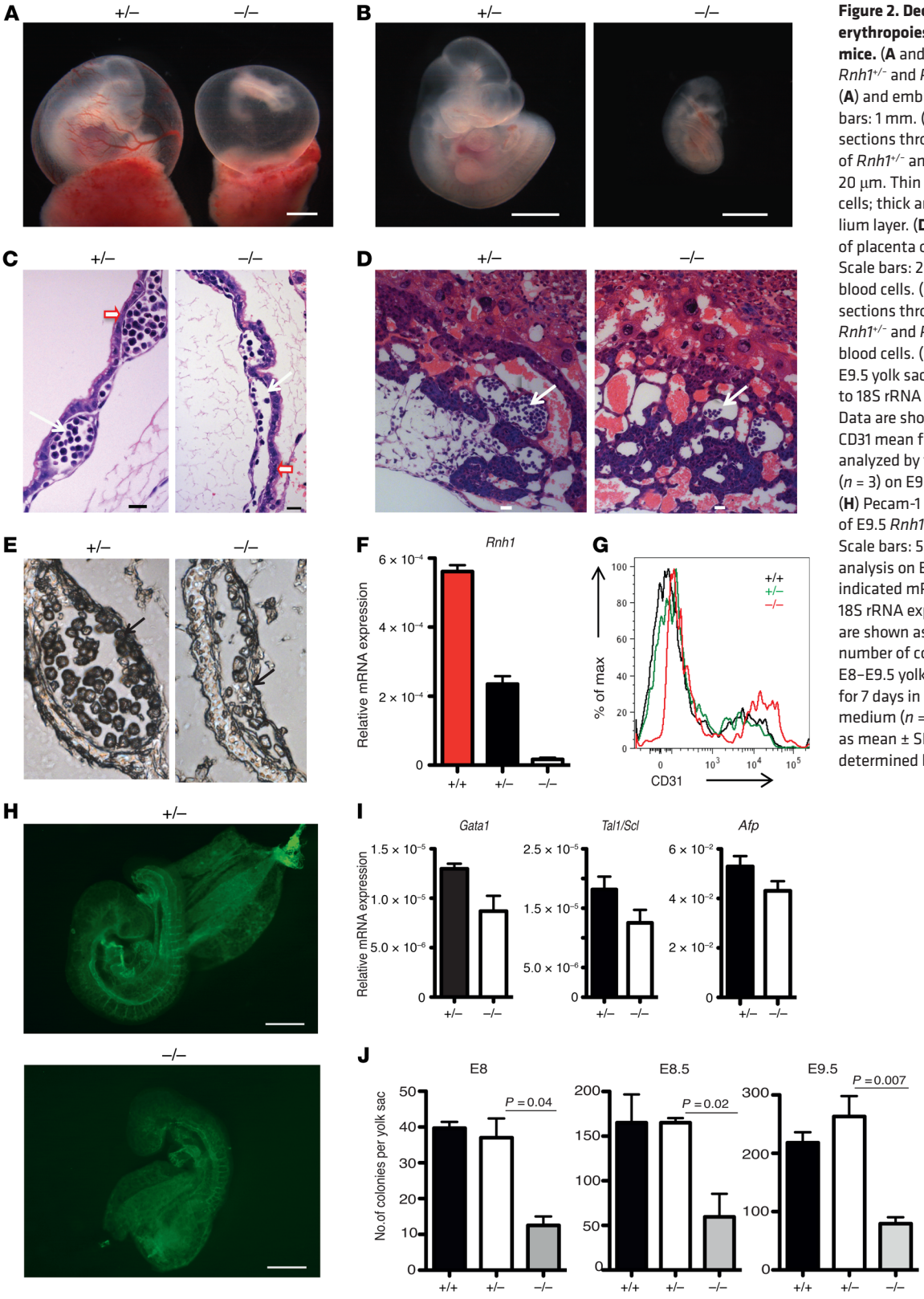

Figure 2. Decreased embryonic erythropoiesis in *Rnh1*-deficient mice. (**A** and **B**) Morphology of E10 *Rnh1*$^{+/-}$ and *Rnh1*$^{-/-}$ whole embryos (**A**) and embryos proper (**B**). Scale bars: 1 mm. (**C**) H&E-stained sections through visceral yolk sacs of *Rnh1*$^{+/-}$ and *Rnh1*$^{-/-}$. Scale bars: 20 μm. Thin arrows indicate blood cells; thick arrows indicate endothelium layer. (**D**) Parasagittal section of placenta of *Rnh1*$^{+/-}$ and *Rnh1*$^{-/-}$. Scale bars: 20 μm. Arrows indicate blood cells. (**E**) Benzidine-stained sections through visceral yolk sac of *Rnh1*$^{+/-}$ and *Rnh1*$^{-/-}$. Arrow indicates blood cells. (**F**) qRT-PCR analysis of E9.5 yolk sac for *Rnh1*, normalized to 18S rRNA expression (n = 3–5). Data are shown as mean ± SEM. (**G**) CD31 mean fluorescence intensity analyzed by flow cytometry (n = 3) on E9.5 total yolk sac cells. (**H**) Pecam-1 (CD31) immunostaining of E9.5 *Rnh1*$^{+/-}$ and *Rnh1*$^{-/-}$ embryos. Scale bars: 500 μm. (**I**) qRT-PCR analysis on E9.5 yolk sac for the indicated mRNAs, normalized to 18S rRNA expression (n = 3–5). Data are shown as mean ± SEM. (**J**) Total number of colonies observed when E8–E9.5 yolk sac cells were cultured for 7 days in methyl cellulose medium (n = 3–4). Data are shown as mean ± SEM. P values were determined by 2-tailed t test.

as *Gata1* mRNA levels were not reduced to the same degree as GATA1 protein levels, an observation based on the markedly decreased ratio of protein to mRNA (Figure 5, D and E). To determine whether decreased GATA1 protein levels reflected impaired translation, we profiled polysomes extracted from yolk sac cells. mRNAs contained in polysomes are bound to multiple ribosome units and actively translated; thus, the measure of polysome-associated mRNAs is an indication of their translation rate (3).

Polysomes were decreased in *Rnh1*$^{-/-}$ cells and, when normalized to 18S rRNA, polysome and monosome fractions contained lower levels of *Gata1* mRNA than those of *Rnh*$^{+/-}$, while mRNA levels of another erythroid TF, *Hoxb4*, remained comparable in *Rnh1*$^{-/-}$ and *Rnh1*$^{+/-}$ polysomes (Figure 5, F and G). These results suggest that, even though the overall translation rate is affected in *Rnh1*$^{-/-}$ cells, *Gata1* mRNA translation is further specifically decreased. Global protein levels were comparable in E10 embryos, as seen with Ponceau S staining (Figure 5C), and also CD31 levels were not decreased in *Rnh1*$^{-/-}$ endothelial cells (Figure 2H). A specific decrease of *Gata1* mRNA translation was also observed in cells deficient for RP RPS19, which is mutated in DBA patients (6). In support of an upstream role of RNH1 in GATA1 expression, transient expression of GATA1 in yolk sac *Rnh1*$^{-/-}$ cells restored the usual frequency of erythroid colonies in a methylcellulose colony-forming assay (Figure 6, A and B, and Supplemental Figure 5). Taken together, these results suggest that RNH1 is required for efficient recruitment of *Gata1* mRNA to the ribosome complex.

RNH1 regulates erythroid differentiation by controlling GATA1 translation in human erythroleukemia K562 cells. We wanted to confirm some of the results obtained in *Rnh1*-deficient mice using a human cell line. For this purpose, we knocked out *RNH1* using the CRISPR/cas9 system in the erythroleukemia cell line K562, which expresses embryonic globin genes (28) (Figure 7A; see complete unedited blots in the supplemental material), and indeed reproduced many of the findings obtained in *Rnh1*$^{-/-}$ mice: *RNH1*-KO cells expressed less GATA1 protein compared with WT cells, even though *GATA1* mRNA levels were similar (Figure 7, A and B). The percentage of benzidine-positive cells was decreased in unstimulated *RNH1*-KO cells (Figure 7C) and in hemin-treated cells (Figure 7D), suggesting a defect in erythroid differentiation. We also found fewer polysomes in *RNH1*-KO cells (Figure 7E) and decreased *GATA1* mRNA abundance in monosome and polysome fractions compared with other investigated erythroid genes (Figure 7F). When cells were labeled for 4 hours with the methionine analogue L-azidohomoalanine (6), less label was incorporated into GATA1 immunoprecipitates from *RNH1*-KO K562 cells than from control cells, further suggesting that GATA1 translation is impaired in the absence of RNH1 (Supplemental Figure 6, A–C; see complete unedited blots in the supplemental material). Furthermore, an RNA-sequencing (RNA-seq) analysis showed significant downregulation of GATA1 target genes in *RNH1*-KO cells compared with WT (Supplemental Figure 7 and Supplemental Table 4). Finally, transient expression of GATA1 in *RNH1*-KO cells restored the usual frequency of benzidine-positive cells, in line with a role of RNH1 upstream of GATA1 expression (Supplemental Figure 8; see complete unedited blots in the supplemental material). Moreover, overexpression of Flag-RNH1 in WT K562 cells increased the relative abundance of polysomes, increased globin mRNA levels, and increased the percentage of benzidine-positive cells (Figure 8, A–E; see complete unedited blots in the supplemental material), further indicating that RNH1 is functional in human K562 cells in a cell-intrinsic manner.

RNH1 is known to inhibit ribonucleases and protect RNA, raising the question of whether this function might contribute to decreasing or increasing polysomes in *RNH1*-deficient or overexpressing cells, respectively. To address this, we checked 28S/18S rRNA ratios and RNA quality and found that both were comparable in RNH1-KO and WT K562 cells (Supplemental Figure 9, A and B). Further, overexpression of an RNH1-mutant (RNH1ΔC) that does not bind to RNase1 also increased polysomes (Supplemental Figure 10, A–C; see complete unedited blots in the supplemental material). These results suggest that polysome stabilization by RNH1 might be independent of its RNAse inhibitor function. A recent study has suggested that GATA1-mutant human erythroid cells in culture failed to upregulate expression of translation apparatus genes (29). In K562 cells, however, ribosome biogenesis and rRNA-processing genes were not reduced in the absence of RNH1 (Supplemental Figure 11, A and B). Overall, these results suggest that RNH1 controls GATA1 translation.

RNH1 regulates erythroid differentiation in primary human CD34^{+} *HSPCs*. We evaluated whether RNH1 also regulates differentiation of primary adult human CD34^{+} HSPCs to the erythroid lineage. In these cells, RNH1 was knocked down using shRNAs and erythroid and myeloid differentiation was induced separately, as shown schematically in Figure 9A. RNH1 knockdown efficiently decreased RNH1 protein levels in CD34^{+} HSPCs (Figure 9B; see complete unedited blots in the supplemental material). Surface expression of CD71 (loss of CD71 indicates erythroid maturation) remained high in RNH1-knockdown cells (Figure 9C and Supplemental Figure 12), suggesting decreased erythroid maturation. RNH1-knockdown cells also showed decreased enucleation, as determined by Hoechst 33342 staining (Figure 9D). Further, morphological analysis of cytospins showed decreased maturation and enucleation in RNH1-knockdown cells (Figure 9F). However, there was no difference in myelopoiesis, as determined by CD16/CD11b FACS staining, and in mature neutrophil numbers (Figure 9, E and F). In differentiated myeloid cells, RNH1 knockdown did not affect mRNA and protein levels of the myeloid TFs PU.1 (SPI1) and C/EBPα (CEBPA) (Figure 9, G and H; see complete unedited blots in the supplemental material). In contrast, GATA1 protein, but not mRNA levels, were decreased in erythroid cells knocked down for RNH1 (Figure 9, I and J; see complete unedited blots in the supplemental material). These results support our previous findings in mice and in human K562 cells that RNH1 controls GATA1 translation and erythroid differentiation.

Interestingly, we also observed decreased protein levels of other erythroid TFs, FOG1 (ZFPM1) and KLF1, in RNH1-knockdown cells (Figure 9, J and K; see complete unedited blots in the supplemental material). mRNA levels of *KLF1* were decreased in RNH1-knockdown cells (Figure 9I). Since GATA1 directly controls KLF1 expression (30, 31), the reduction in GATA1 levels may explain decreased mRNA and protein levels of KLF1. In the case of FOG1, similarly to what occurred with GATA1, mRNA levels were not decreased in RNH1-knockdown cells, suggesting that RNH1 might also control FOG1 translation. Overall, these results suggest that RNH1 regulates erythropoiesis and can control GATA1 translation in human CD34^{+} progenitors. RNH1 may also control translation of other genes that affect erythropoiesis.

RNH1 is present in ribosome fractions and binds to the small ribosomal subunit. We next wondered how RNH1 was molecularly connected to the translation machinery. In K562 lysates, although the majority of RNH1 was found in a postribosomal fraction (S100), RNH1 was also detected in a polysome-enriched fraction (P100)

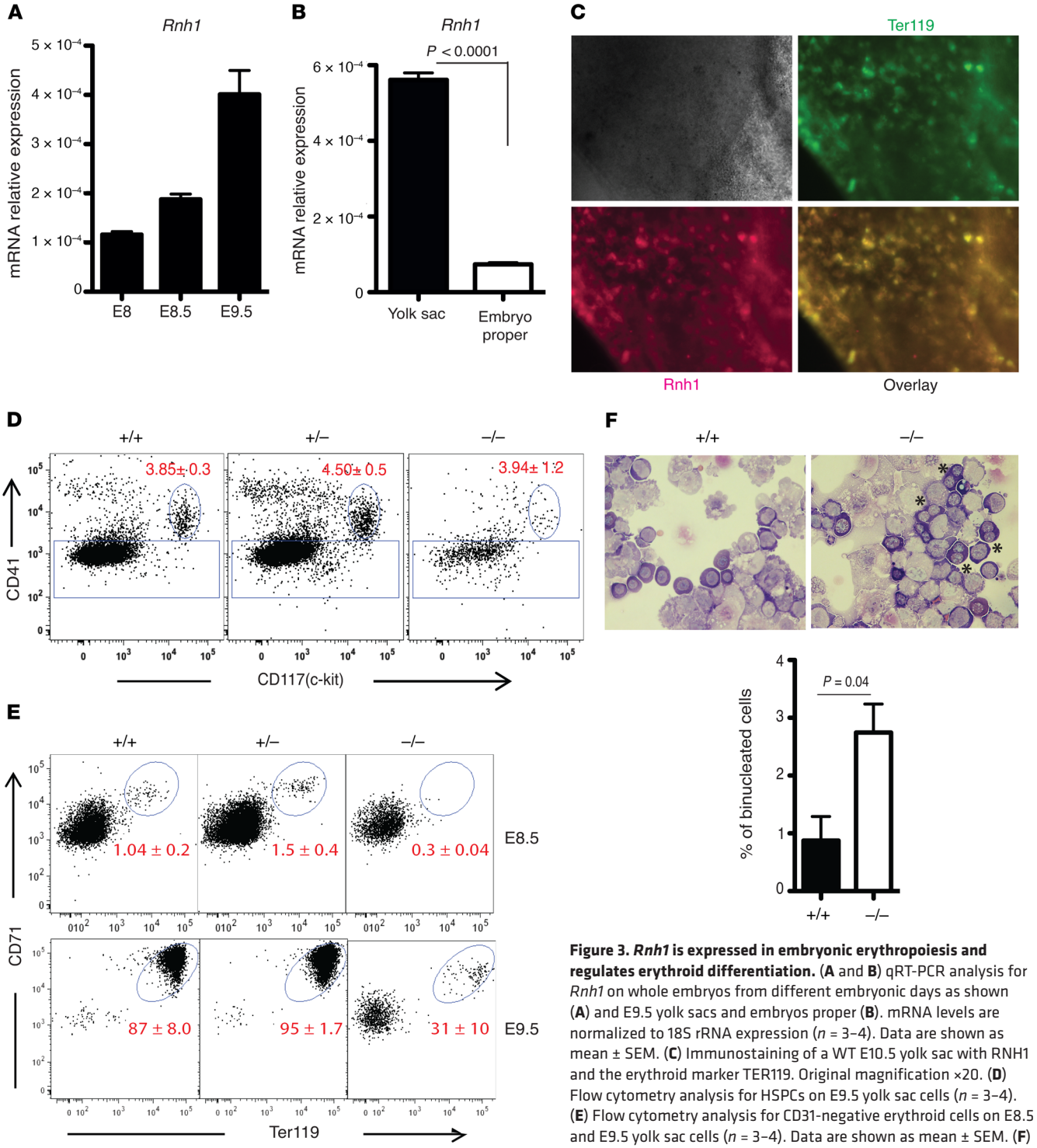

Figure 3. *Rnh1* is expressed in embryonic erythropoiesis and regulates erythroid differentiation. (**A** and **B**) qRT-PCR analysis for *Rnh1* on whole embryos from different embryonic days as shown (**A**) and E9.5 yolk sacs and embryos proper (**B**). mRNA levels are normalized to 18S rRNA expression (n = 3–4). Data are shown as mean ± SEM. (**C**) Immunostaining of a WT E10.5 yolk sac with RNH1 and the erythroid marker TER119. Original magnification ×20. (**D**) Flow cytometry analysis for HSPCs on E9.5 yolk sac cells (n = 3–4). (**E**) Flow cytometry analysis for CD31-negative erythroid cells on E8.5 and E9.5 yolk sac cells (n = 3–4). Data are shown as mean ± SEM. (**F**) Cytospins from yolk sac cells were stained with Pappenheim stain (left). Binucleated erythroblasts are indicated by asterisks. Representative bar graph showing percentage of binucleated cells (right) (n = 3). Original magnification ×400. Data are shown as mean ± SEM. P values were determined by 2-tailed t test.

(Figure 10A; see complete unedited blots in the supplemental material) and in the polysome fractions of a sucrose gradient (Figure 10B; see complete unedited blots in the supplemental material). After high-salt (0.5 M KCl) treatment, some RNH1 remained associated with the 80S monosome fraction (Figure 10C; see complete unedited blots in the supplemental material), while after puromycin-induced dissociation of ribosomes into 40S and 60S subunits (32), RNH1 was found associated to the 40S subunit (Figure 10D; see complete unedited blots in the supplemental material). The salt conditions used in this experiment are known to remove translation factors that

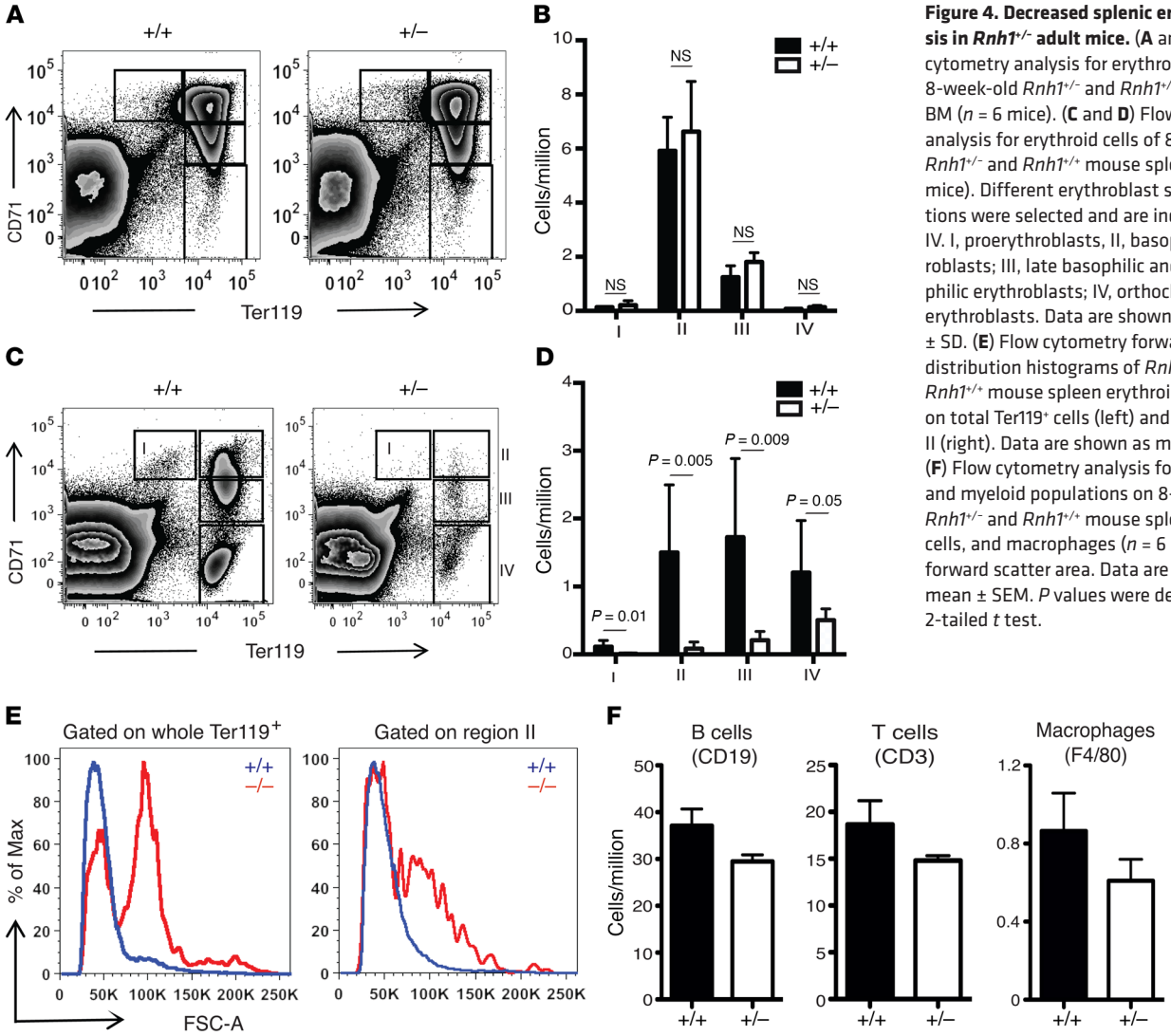

Figure 4. Decreased splenic erythropoiesis in *Rnh1*$^{+/-}$ adult mice. (**A** and **B**) Flow cytometry analysis for erythroid cells of 8-week-old *Rnh1*$^{+/-}$ and *Rnh1*$^{+/+}$ mouse BM (n = 6 mice). (**C** and **D**) Flow cytometry analysis for erythroid cells of 8-week-old *Rnh1*$^{+/-}$ and *Rnh1*$^{+/+}$ mouse spleens (n = 6 mice). Different erythroblast subpopulations were selected and are indicated as I to IV. I, proerythroblasts, II, basophilic erythroblasts; III, late basophilic and chromatophilic erythroblasts; IV, orthochromatophilic erythroblasts. Data are shown as mean ± SD. (**E**) Flow cytometry forward-scatter distribution histograms of *Rnh1*$^{+/-}$ and *Rnh1*$^{+/+}$ mouse spleen erythroid cells gated on total Ter119^{+} cells (left) and on region II (right). Data are shown as mean ± SD. (**F**) Flow cytometry analysis for lymphoid and myeloid populations on 8-week-old *Rnh1*$^{+/-}$ and *Rnh1*$^{+/+}$ mouse spleen B cells, T cells, and macrophages (n = 6 mice). FSC-A, forward scatter area. Data are shown as mean ± SEM. P values were determined by 2-tailed t test.

associate with ribosomes, aminoacyl-tRNA synthetases, and some protein kinases, but not intrinsic RPs (32). These results suggest that RNH1 can directly interact with the small ribosomal subunit. In order to confirm the interaction of RNH1 with ribosomes, Flag-RNH1 was immunoprecipitated from transfected or untransfected K562 cells and interacting proteins were identified by mass spectrometry (MS) (Supplemental Table 5). RPs and proteins involved in RNA processing were among the top enriched functional categories that bound to RNH1 (Figure 11A). This was confirmed by Western blot for RPs RPL11 and RPS3, while 2 proteins not found in the MS analysis, the ribosome protein RPS6 and the elongation factor EEF2, were negative by Western blot in the Flag-RNH1 immunoprecipitate (Figure 11B; see complete unedited blots in the supplemental material). Further supporting these data, RNH1 was present in a recently analyzed mammalian riboproteome (33). Collectively, these results indicate that RNH1 interacts with RPs and support the role of RNH1 in translation and erythropoiesis.

Discussion

RNH1 is known to inhibit ribonucleases and protect RNA from degradation. However, the precise biological role of RNH1 in vivo remains unexplored. Our results have uncovered a crucial function for RNH1 in the regulation of erythropoiesis by controlling GATA1 translation. Embryonic erythropoiesis starts between E7 and E7.5 by producing primitive erythroid cells from a transient wave of committed progenitors in the yolk sac (16). These primitive erythroid cells support the rapid growth of the embryo during early embryonic development. We demonstrate that *Rnh1* expression localizes to erythroid cells at the onset of primitive erythropoiesis and that *Rnh1* deficiency resulted in a lethal decrease in erythroid differentiation and the hemoglobin content per cell. The anemia phenotype observed in *Rnh1*$^{-/-}$ embryos was not associated with defective vasculogenesis and HSPC generation, since blood vessel formation and HSPC generation were intact. Further, *Rnh1* haploinsufficiency decreased adult erythropoiesis in the spleen, further pointing to the importance of *Rnh1* in maintaining erythropoiesis.

Similarly, RNH1 deficiency in human K562 cells and RNH1 knockdown in primary CD34^{+} HSPCs reduced erythroid differentiation, suggesting that its role is conserved across species and that it can play a cell-intrinsic function. Interestingly, the transcriptome of *Rnh1*$^{-/-}$ yolk sac cells revealed that the expression levels of erythroid TFs were not deficient, but that their target genes were

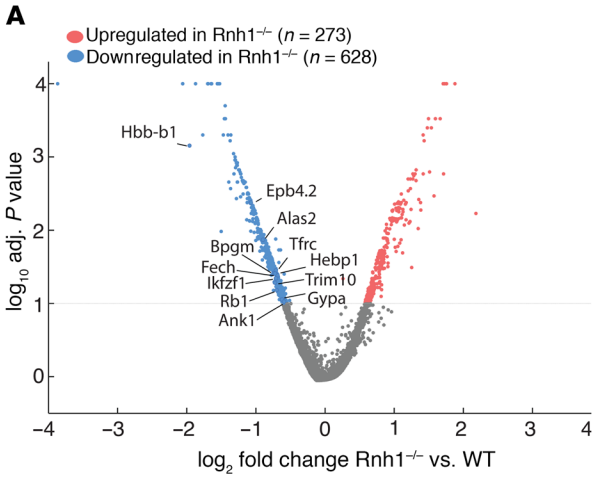
A
Upregulated in Rnh1−/− (n = 273)
Downregulated in Rnh1−/− (n = 628)
log10 adj. P value
log2 fold change Rnh1−/− vs. WT
Hbb-b1
Epb4.2
Alas2
Bpgm
Tfrc
Fech
Hebp1
Ikfzf1
Trim10
Rb1
Gypa
Ank1

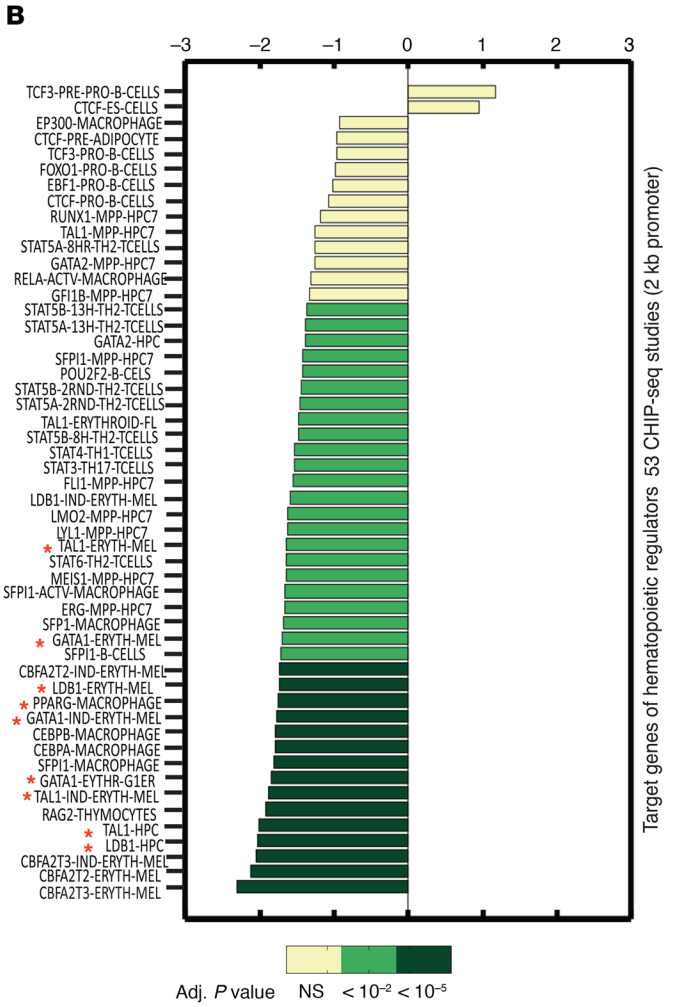
B
TCF3-PRE-PRO-B-CELLS
CTCF-ES-CELLS
EP300-MACROPHAGE
CTCF-PRE-ADIPOCYTE
TCF3-PRO-B-CELLS
FOXO1-PRO-B-CELLS
EBF1-PRO-B-CELLS
CTCF-PRO-B-CELLS
RUNX1-MPP-HPC7
TAL1-MPP-HPC7
STAT5A-8HR-TH2-TCELLS
GATA2-MPP-HPC7
RELA-ACTV-MACROPHAGE
GFI1B-MPP-HPC7
STAT5B-13H-TH2-TCELLS
STAT5A-13H-TH2-TCELLS
GATA2-HPC
SFPI1-MPP-HPC7
POU2F2-B-CELS
STAT5B-2RND-TH2-TCELLS
STAT5A-2RND-TH2-TCELLS
TAL1-ERYTHROID-FL
STAT5B-8H-TH2-TCELLS
STAT4-TH1-TCELLS
STAT3-TH17-TCELLS
FLI1-MPP-HPC7
LDB1-IND-ERYTH-MEL
LMO2-MPP-HPC7
LYL1-MPP-HPC7
TAL1-ERYTH-MEL
STAT6-TH2-TCELLS
MEIS1-MPP-HPC7
SFPI1-ACTV-MACROPHAGE
ERG-MPP-HPC7
SFP1-MACROPHAGE
GATA1-ERYTH-MEL
SFPI1-B-CELLS
CBFA2T2-IND-ERYTH-MEL
LDB1-ERYTH-MEL
PPARG-MACROPHAGE
GATA1-IND-ERYTH-MEL
CEBPB-MACROPHAGE
CEBPA-MACROPHAGE
SFPI1-MACROPHAGE
GATA1-EYTHR-G1ER
TAL1-IND-ERYTH-MEL
RAG2-THYMOCYTES
TAL1-HPC
LDB1-HPC
CBFA2T3-IND-ERYTH-MEL
CBFA2T2-ERYTH-MEL
CBFA2T3-ERYTH-MEL
Target genes of hematopoietic regulators 53 CHIP-seq studies (2 kb promoter)
Adj. P value NS < 10−2 < 10−5

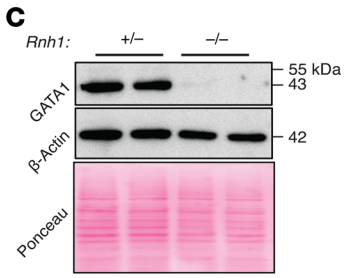
C
Rnh1: +/− −/−
GATA1
β-Actin
Ponceau
55 kDa
43
42

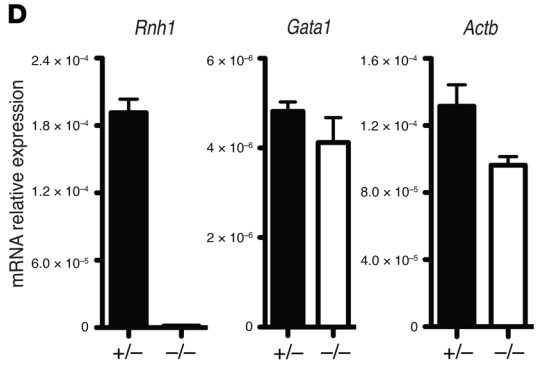
D
Rnh1
Gata1
Actb
mRNA relative expression
+/− −/−

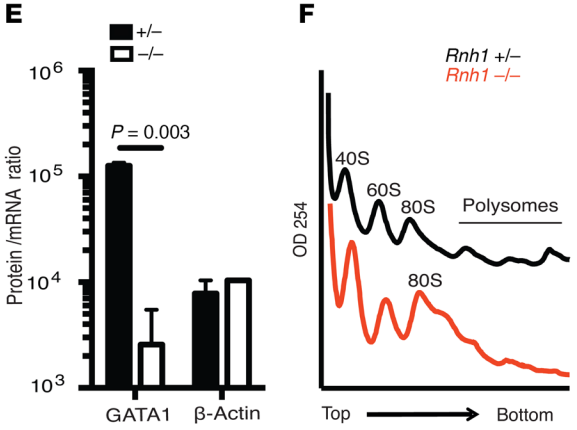
E
+/−
−/−
P = 0.003
Protein /mRNA ratio
GATA1
β-Actin
F
Rnh1 +/−
Rnh1 −/−
40S
60S
80S
Polysomes
OD 254
Top
Bottom

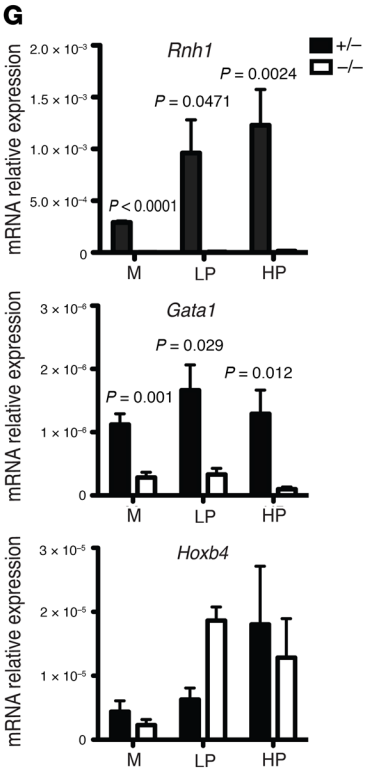
G
Rnh1
P = 0.0024
P = 0.0471
P < 0.0001
Gata1
P = 0.029
P = 0.012
P = 0.001
Hoxb4
mRNA relative expression
M
LP
HP

Figure 5. RNH1 deficiency decreases GATA1 protein levels. (**A**) Up- and downregulated genes of E9.5 yolk sacs from *Rnh1*$^{-/-}$ mice compared with WT (probability of false positive < 0.1). Adj, adjusted. (**B**) Target enrichment analysis of essential erythroid TF targets in E9.5 yolk sacs from *Rnh1*$^{-/-}$ mice. Bars correspond to the GSEA normalized enrichment scores of target sets extracted from a collection of ChIP-seq studies (n = 52). NS corresponds to an adjusted P value of greater than 0.01. Asterisks indicate key regulators of erythropoiesis. (**C**) Western blot analysis of total protein lysates isolated from E10 embryos, using indicated antibodies. Nitrocellulose membranes were stained with Ponceau S to demonstrate protein loading. Blots are representative of 3 independent experiments. (**D**) qRT-PCR analysis of E10 embryos for indicated mRNAs, normalized to 18S rRNA (n = 3). Data are shown as mean ± SEM. (**E**) Protein/mRNA ratios were determined using densitometric values of proteins, and 18S rRNA–normalized mRNA expression values for E10 total embryos. Data are expressed as mean ± SD. (**F**) Sucrose gradient polysome profiles for *Rnh1*$^{+/-}$ and *Rnh1*$^{-/-}$ yolk sac–derived cells from E10 embryos. Arrow shows the direction of the sucrose gradient from low to high density. Data are representative of 3 independent experiments. (**G**) qRT-PCR analysis for indicated mRNAs in monosome (M), light polysome (LP), and heavy polysome (HP) fractions derived from E10 *Rnh1*$^{+/-}$ and *Rnh1*$^{-/-}$ yolk sac cells. mRNA levels were normalized to 18S rRNA expression. Data are shown as mean ± SEM. Data are representative of 3 independent experiments. P values were determined by 2-tailed t test.

reduced. This is in line with our observation that RNH1 associates with RPs to favor polysome formation and enhance translation. Supporting this, *GATA1* mRNA levels were not affected, but protein levels were decreased. Further, transient expression of GATA1 in RNH1-deficient mouse yolk sac cells and K562 cells restored the erythroid differentiation defect observed in *RNH1*-deficient cells, suggesting a role of RNH1 upstream of GATA1 expression.

Mutations in RPs interfere with ribosome biogenesis, which is considered as the main pathological mechanism for DBA (4). DBA is a rare congenital pure red cell aplasia characterized by anemia, macrocytosis, and reticulocytopenia (4). In DBA patients, mutation of RPs, such as RPS19, leads to impaired ribosomal biogenesis and causes a defect in translation of GATA1 and erythroid-related genes (5, 6). Similarly, RNH1 is a ribosome-associated protein expressed by erythroid cells whose deficiency caused decreased GATA1 translation and defective differentiation of erythroid cells (Figure 12). Defects in ribosomal biogenesis can lead to TP53 upregulation and apoptosis (34). Nonetheless, impaired erythropoiesis in *Rnh1*-deficient embryos was not associated with p53-dependent apoptosis, since we did not find TP53 upregulation or enrichment of TP53-related apoptotic genes (Supplemental Table 1). Although this work focused mainly on GATA1, we consider it likely that RNH1 regulates translation of other erythroid-specific genes. Determining precisely how this specific regulation of translation takes place requires further investigation. RNH1 is only present in vertebrates and was proposed to be an intracellular sentry, since it protects cytosolic RNA from extracellular ribonucleases (35). However, our combined functional and systems-level analyses show that this is not the sole or perhaps even the main function of RNH1 in vivo. In conclusion, we present a function for RNH1 in GATA1 translation and erythropoiesis. These data add RNH1 to the list of ribosomal-associated factors that regulate specific mRNA translation (1). This warrants further studies on RNH1 and may provide novel therapeutic opportunities for erythropoiesis-related disorders.

Methods

Generation of Rnh1$^{-/-}$ *mice*. Rnh1 targeting vector (Figure 1A) was electroporated into hybrid (C57BL/6 × 129/SvEv) embryonic stem (ES) cells. Homologous recombinant ES cells were identified by Southern blot analysis and microinjected into blastocysts. Offspring were backcrossed to C57BL/6 mice, and germline transmission was confirmed by PCR of tail genomic DNA. Screening of *Rnh1*-deficient mice by PCR genotyping was carried out using the following primers on embryo or ear genomic DNA: 5′-CTGATAACTTATTTCCGGGATAC (forward in intron 1), 5′-ACCACTTCGTATTGCTGGA (reverse in exon 2), and 5′-TAAGCTTGGATCCGTTCTTC (reverse in PGK-NEO cassette). We used 8-week-old male *Rnh1*$^{+/+}$ and *Rnh*$^{+/-}$ mice (n = 6 mice) to analyze different cell populations in spleen and BM.

RNA preparation and qRT-PCR. Total RNA was isolated from embryos, yolk sacs, and K562 cells using the QIAGEN RNeasy Kit according to the manufacturer's protocol. Reverse transcription and real-time PCR (RT-PCR) from total RNA was carried out as described previously (36). The SYBR Green Dye detection system was used for quantitative real-time PCR on Light Cycler 480 (Roche). Gene-specific primers (Microsynth) used are listed in Supplemental Table 6. Controls consisting of ddH_2O were negative for target and housekeeping genes.

Gene expression analysis. Total RNA from E9.5 yolk sacs of different genotypes (*Rnh1*$^{+/+}$, *Rnh1*$^{+/-}$, and *Rnh1*$^{-/-}$) was isolated and purified with the QIAGEN RNeasy Kit according to the manufacturer's protocol. All RNA amounts were monitored with a NanoDrop ND-1000 spectrophotometer, and the RNA quality was assessed using RNA 6000 NanoChips with the Agilent 2100 Bioanalyzer. For each sample, 100 ng of total RNA was amplified using the WT Sense Strand Target Labelling Kit (Affymetrix, catalog 900223); 5.5 μg of the resulting sense cDNA was fragmented by uracil DNA glycosylase (UDG) and apurinic/apyrimidic endonuclease 1 (APE 1) and biotin-labeled with terminal deoxynucleotidyl transferase (TdT) using the GeneChip WT Terminal Labelling Kit (Affymetrix, 900671). Affymetrix Mouse Gene 1.0 ST arrays were hybridized with 2.7 μg of biotinylated target at 45°C for 17 hours and washed and stained according to the protocol described the in the Affymetrix GeneChip Expression Analysis Manual (Fluidics protocol FS450_0007). The arrays were scanned using GeneChip Scanner 3000 7G (Affymetrix), and raw

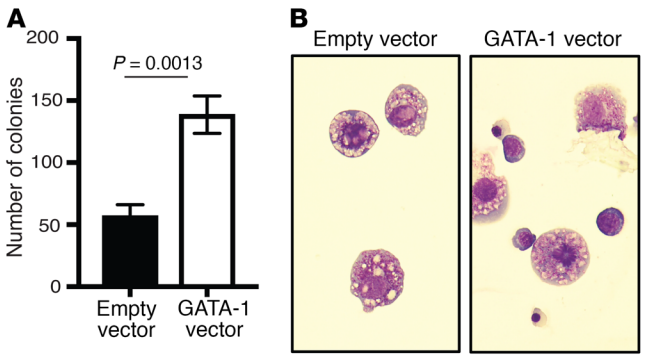

Figure 6. GATA1 overexpression rescues erythroid phenotype in Rnh1-deficient yolk sac cells. (**A**) Total number of colonies observed in control and GATA1- infected Rnh1-deficient yolk sac cells that were cultured for 7 days in methyl cellulose medium (n = 3). Data are shown as mean ± SD. P values were determined by 2-tailed t test. (**B**) Cytospin images of erythroid cells derived from methyl cellulose colonies of control and GATA1-infected cells. More mature erythroid cells were observed in GATA1-infected cells. Original magnification ×400.

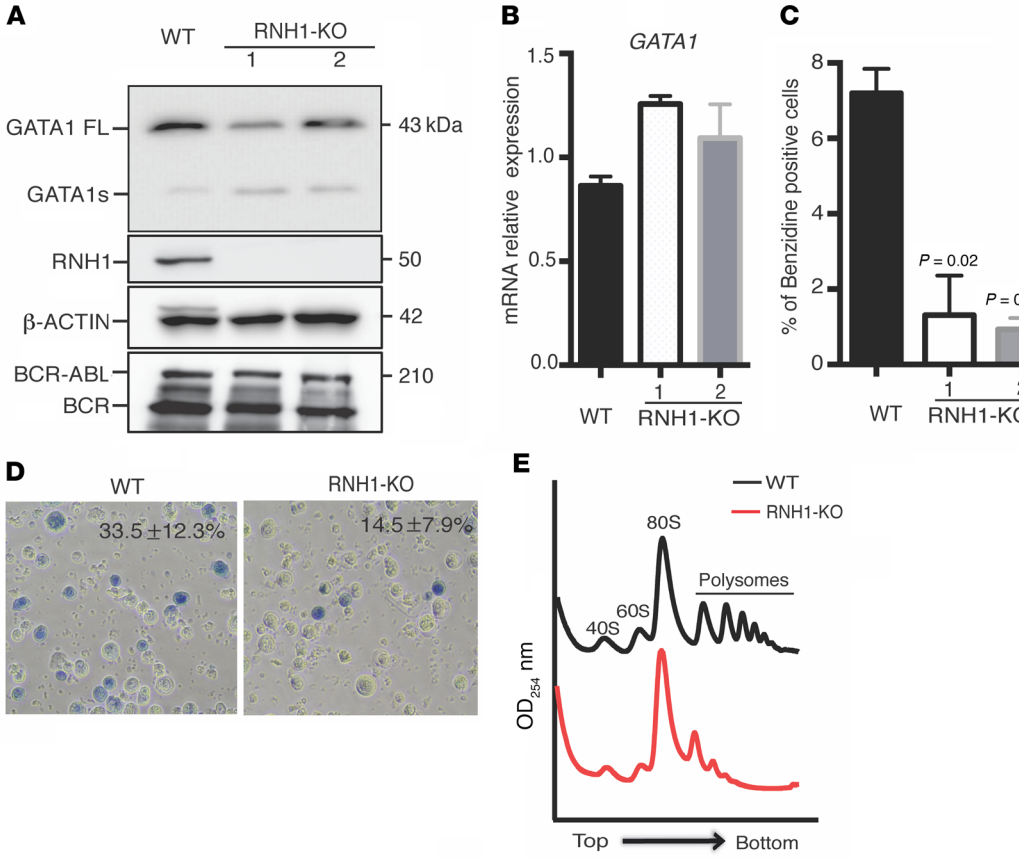

Figure 7. RNH1 deficiency decreases erythroid differentiation and GATA1 protein levels in K562 cell. (**A**) Total protein lysates of WT and *RNH1*-KO K562 cells were analyzed by Western blot with the indicated antibodies. K562 cells were positive for BCR-ABL oncogene. Blots are representative of 3 independent experiments. (**B**) qRT-PCR analysis for *GATA1* mRNA levels in K562 cells, normalized to 18S rRNA expression. Data are shown as mean ± SD and are representative of 3 independent experiments. (**C**) Number of benzidine-positive K562 cells. Data are shown as mean ± SD and are representative of 3 independent experiments. (**D**) K562 cells were treated with hemin (25 μM) for 3 days and analyzed for the presence of benzidine-positive cells. Data are shown as mean ± SD and are representative of 3 independent experiments. Original magnification ×200. (**E**) Polysome profiles for WT and *RNH1*-KO K562 cells. Data are representative of 3 independent experiments. (**F**) qRT-PCR analysis for indicated mRNAs in monosome and polysome fractions derived from WT and *RNH1*-KO K562 cells, normalized to 18S rRNA expression. Data are shown as mean ± SD and are representative of 3 independent experiments. *P* values were determined by 2-tailed *t* test.

data were extracted from the scanned images and analyzed with the Affymetrix Power Tools software package. Affymetrix Hybridization quality was assessed using Expression Console software (Affymetrix). Microarray analysis was performed using various Bioconductor packages in the R environment (http://www.bioconductor.org). Normalized expression signals were calculated from Affymetrix CEL files using the RMA normalization implemented in the Affy package (37), and differential expression analysis was performed using the Rank Products package (38).

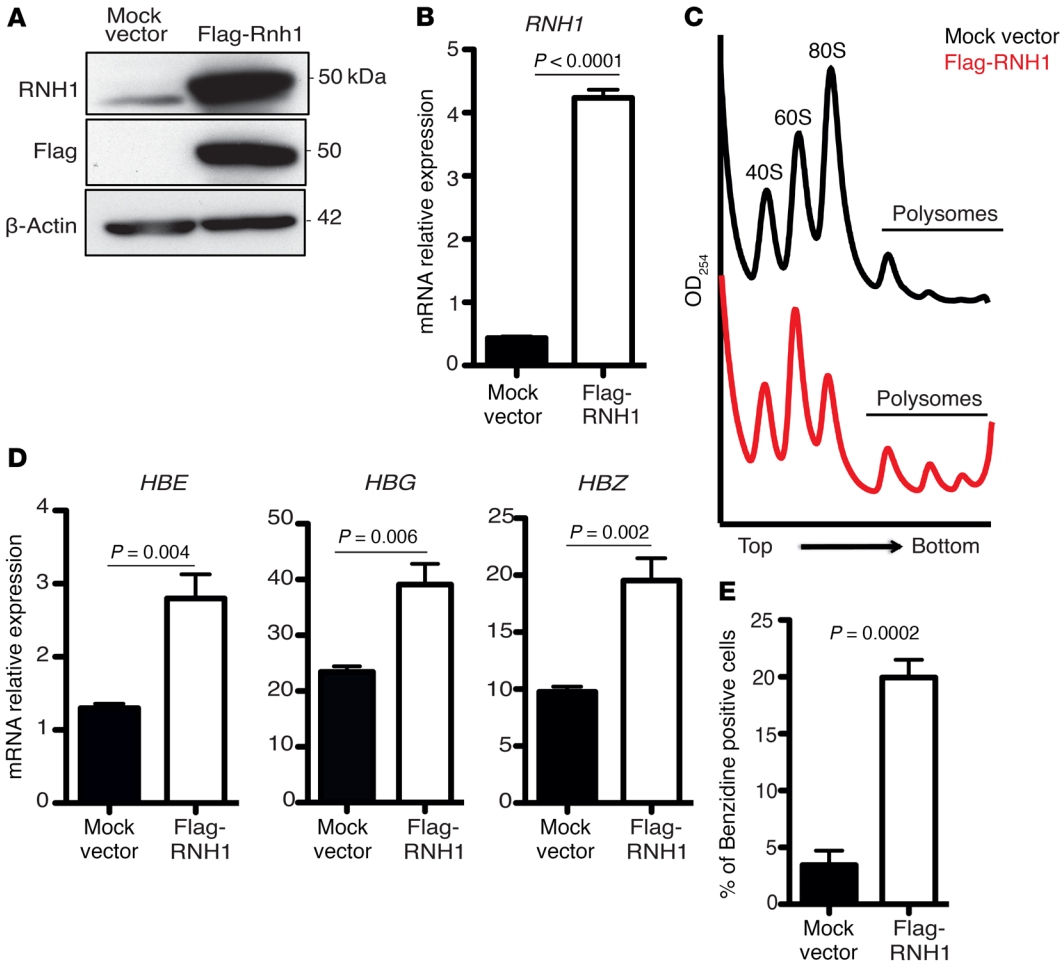

Figure 8. RNH1 induces globin gene expression in K562 cells. (**A**) RNH1 expression in stable K562 cells expressing mock or Flag-RNH1 vector by Western blot. Blots are representative of 2 to 3 independent experiments. (**B**) RNH1 expression in stable K562 cells expressing mock or Flag-RNH1 vector by qRT-PCR. Relative mRNA expression was normalized to HPRT expression. Data are shown as mean ± SEM. Data are representative of 3 independent experiments. (**C**) Sucrose gradient polysome profiles for mock- or RNH1-expressing stable K562 cells. Arrows show direction of the sucrose gradient from less to more dense. Data are representative of 3 independent experiments. (**D**) qRT-PCR analysis for globin genes in stable K562 cells expressing mock or Flag-RNH1 vector. Data expressed mRNA levels normalized to *HPRT* expression. Data are shown as mean ± SEM. (**E**) Percentage of benzidine-positive cells in mock or Flag-RNH1 vector–expressing stable K562 cells. Data are shown as mean ± SEM. Data are representative of 3 independent experiments. *P* values were determined by 2-tailed *t* test.

Phenotype enrichment analysis. We applied the Phenotype Ontology Enrichment program available in the MouseMine database (http://www.mousemine.org/mousemine/begin.do) to determine phenotypes significantly enriched among downregulated genes in *Rnh1*$^{-/-}$ mice. Enriched phenotypes are related to spontaneous, chemically induced, or targeted mutations of mouse genes. The complete list of significant phenotypes (Benjamini-Hochberg adjusted *P* values < 0.05) is found in Supplemental Table 2.

Target enrichment analysis. The collection of 52 ChIP-seq studies was obtained from the HemoChIP compendium (39). For each ChIP-seq study, we extracted a list of targets by selecting genes containing at least 1 binding site for the TF in the 2 kb region around the transcription start site. The GSEA test statistic (40) was used to determine upregulation or downregulation of TF targets in *Rnh1*$^{-/-}$ mice. Complete GSEA results and target gene sets are available in Supplemental Table 3.

Hematopoietic colony formation assays. E8, E8.5, and E9.5 yolk sacs were dissected without contamination from maternal tissue under sterile conditions from *Rnh1*$^{+/+}$, *Rnh1*$^{+/-}$, and *Rnh1*$^{-/-}$ embryos. Cells were isolated from yolk sacs by treatment with 0.1% collagenase in PBS and 20% fetal calf serum for 30 minutes at 37°C before mechanical disaggregation, as described previously (20). Total yolk sac cells were cultured for 7 days in methylcellulose semisolid medium containing all essential growth factors that support growth of erythroid progenitors (M3436, Stem Cell Technologies).

Flow cytometry and cell sorting. Single-cell suspensions were prepared from mouse yolk sac and adult BM or spleen. Cells were stained with monoclonal antibodies specific for CD41 (clone MWReg30), CD117 (clone 2B8), CD31 (clone 390), Ter119 (clone TER-119), CD71 (clone R17217), F4/80 (clone BM8), CD11b (clone M1/70), CD19 (clone eBio1D3), and CD3 (clone 17A2). All antibodies were purchased as FITC, phycoerythrin (PE), PE-Cy5, PE-Cy7, APC–eFluor 780, Alexa Fluor 700, or PerCP–eFluor 710 conjugates from eBiosciences. Cells were either acquired on a BD LSRII Flow Cytometer or sorted on a FACSAria I Cell Sorter (BD Biosciences). Data were analyzed with FlowJo (version 9.3.1, TreeStar Inc.) software. For human

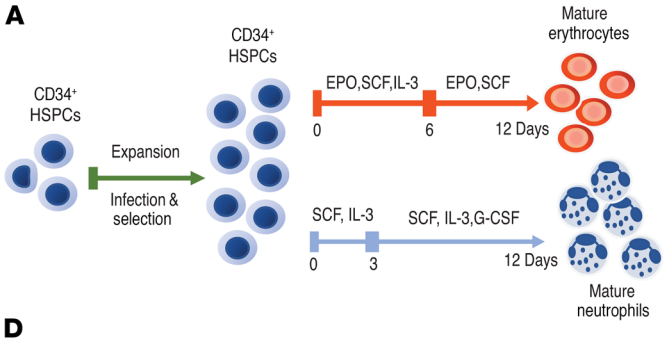
A
CD34+ HSPCs
Expansion
Infection & selection
CD34+ HSPCs
EPO,SCF,IL-3
EPO,SCF
0
6
12 Days
Mature erythrocytes
SCF, IL-3
SCF, IL-3,G-CSF
0
3
12 Days
Mature neutrophils

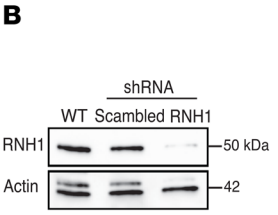
B
shRNA
WT Scrambled RNH1
RNH1
Actin
50 kDa
42

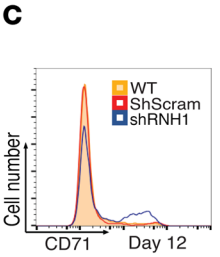
C
WT
ShScram
shRNH1
Cell number
CD71
Day 12

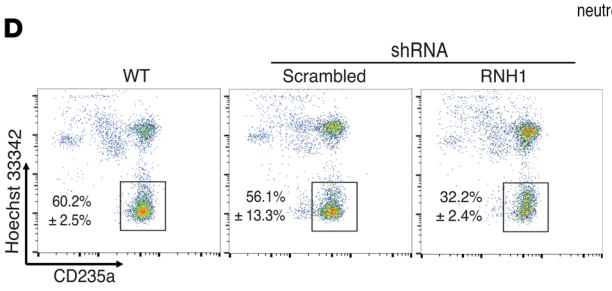
D
shRNA
WT
Scrambled
RNH1
Hoechst 33342
CD235a
60.2% ± 2.5%
56.1% ± 13.3%
32.2% ± 2.4%

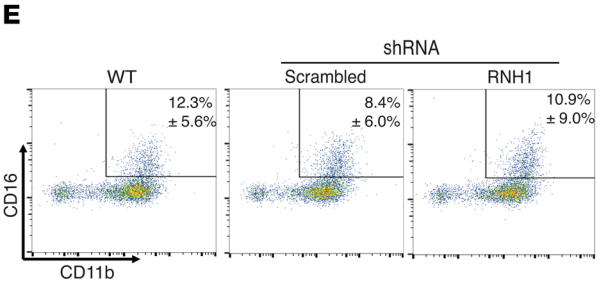
E
shRNA
WT
Scrambled
RNH1
12.3% ± 5.6%
8.4% ± 6.0%
10.9% ± 9.0%
CD16
CD11b

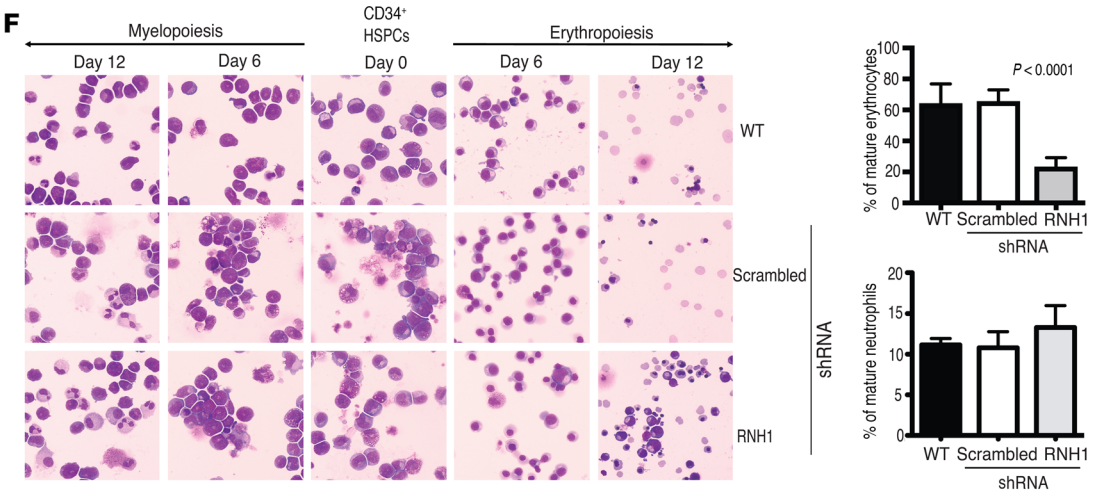
F
Myelopoiesis
CD34+ HSPCs
Erythropoiesis
Day 12
Day 6
Day 0
Day 6
Day 12
WT
Scrambled
RNH1
shRNA
% of mature erythrocytes
P < 0.0001
WT Scrambled RNH1
shRNA
% of mature neutrophils
WT Scrambled RNH1
shRNA

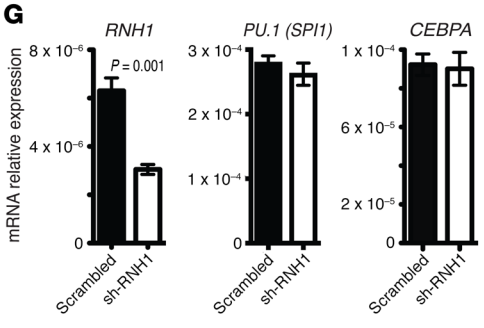
G
RNH1
PU.1 (SPI1)
CEBPA
mRNA relative expression
P = 0.001
Scrambled
sh-RNH1

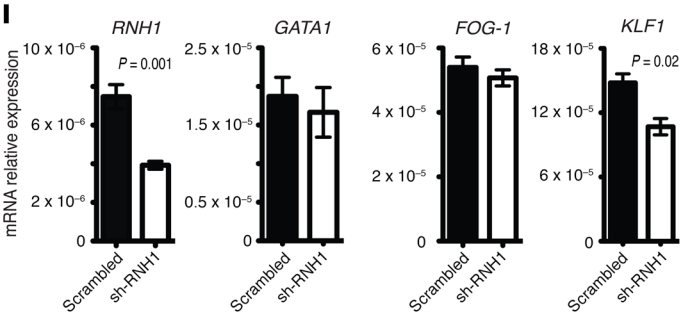
I
RNH1
GATA1
FOG-1
KLF1
mRNA relative expression
P = 0.001
P = 0.02
Scrambled
sh-RNH1

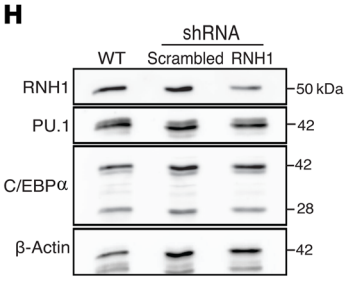
H
shRNA
WT Scrambled RNH1
RNH1
PU.1
C/EBPα
β-Actin
50 kDa
42
42
28
42

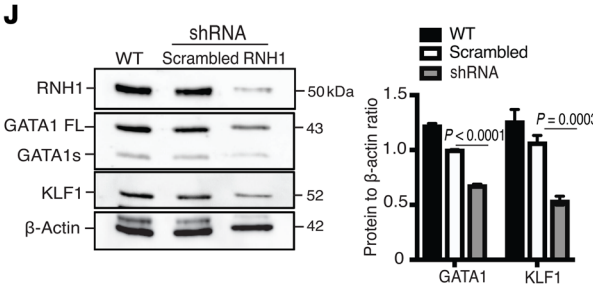
J
shRNA
WT Scrambled RNH1
RNH1
GATA1 FL
GATA1s
KLF1
β-Actin
50 kDa
43
52
42
WT
Scrambled
shRNA
Protein to β-actin ratio
P < 0.0001
P = 0.0003
GATA1
KLF1

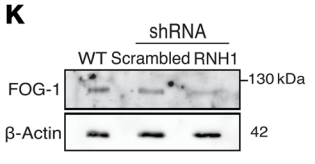
K
shRNA
WT Scrambled RNH1
FOG-1
β-Actin
130 kDa
42

Figure 9. RNH1 knockdown decreases GATA1 protein levels and erythroid differentiation in primary human CD34⁺ HSPCs. (**A**) Schematic illustration showing differentiation of human CD34⁺ HSPCs into mature erythrocytes and neutrophils. (**B**) Western blot analysis of RNH1 in CD34⁺ HSPCs after 4 days of transduction. (**C**) Representative histogram plot showing CD71 surface expression on day 12 of erythroid differentiation (n = 3). shScram, ShRNA Scrambled. (**D**) Flow cytometry analysis for CD235a⁺ and Hoechst 33342⁻ erythrocytes on day 12 of differentiation (n = 3). Data are shown as mean ± SD. (**E**) Flow cytometry analysis for CD11b⁺ and CD16⁺ neutrophils on day 12 of differentiation (n = 3). Data are shown as mean ± SD. (**F**) Cytospin images of erythroid (right) and myeloid (left) differentiated cells at the indicated days of differentiation, stained with May-Grünwald-Giemsa. Representative bar graph on the left shows percentage of morphologically mature erythrocytes (upper panel) and mature neutrophils (lower panel) at day 12 of differentiation (n = 3). Data are shown as mean ± SD. Original magnification ×400. (**G**) qRT-PCR analysis for indicated mRNAs in scrambled and RNH1-knockdown myeloid cells at day 6 of differentiation (n = 3), normalized to 18S rRNA expression. Data are shown as mean ± SD. (**H**) Total protein lysates of scrambled and RNH1 knockdown myeloid cells at day 6 of differentiation were analyzed by Western blot with the indicated antibodies. (**I**) qRT-PCR analysis for indicated mRNA expression in scrambled and RNH1-knockdown erythroid cells at day 6 of differentiation (n = 3) normalized to 18S rRNA expression. Data are shown as mean ± SD. (**J** and **K**) Total protein lysates of scrambled and RNH1-knockdown erythroid cells at day 6 of differentiation were analyzed by Western blot with the indicated antibodies. Right side in figure **J**, densitometric analysis for proteins by ImageJ (NIH). Values were normalized to β-actin. Data are expressed as mean ± SD (right). All blots are representative of 3 independent experiments. P values were determined by 2-tailed t test.

CD34⁺ differentiation experiments, cells were stained with anti-human monoclonal antibodies specific for CD11b (clone ICRF44), CD13 (clone WM-15), CD16 (clone eBioCB16), CD71 (clone OKT9), and CD235a (clone HIR2, also GA-R2). All antibodies were purchased as FITC, PE, or APC from eBiosciences. CD34 (clone AC136) antibody was from Miltenyi Biotec. Hoechst 33342 fluorescent nuclear stain (ImmunoChemistry Technologies) was added at a dilution of 1:200 at least 15 minutes before analysis. Data were acquired on a CytoFLEX S Flow Cytometer (Beckman Coulter). Data analysis was carried out with FlowJo 10.2 (FlowJo LLC).

Immunostaining. Embryos and yolk sacs were fixed with 4% PFA in PBS for 2 hours and then washed with PBST (PBS + 0.3% Triton X-100). After washing, embryos were blocked for 4h with blocking buffer (contains 5% donkey serum and 0.5% BSA in PBS), and then incubated with primary antibody either Pecam-1 (clone MEC 13.3) (BD Bioscience) or RNH1 (catalog H00006050-D01P, Abnova) and Ter119 (catalog 14-5921-82, eBioscience) in blocking buffer overnight at 4°C. After washing with PBST, embryos were incubated overnight with Alexa Fluor secondary antibodies (Invitrogen) in blocking buffer and rinsed with PBST. Microscopy analyses were carried out using a Leica Stereomicroscope or a Time Lapse Inverted Microscope (Axio Observer.Z1).

Immunoblotting. Total mouse embryo-derived cells, human K562 cells, CD34⁺ progenitor cells, erythroid cells, and myeloid cells were resuspended in lysis buffer (20 mM Tris, pH 7.4, 150 mM NaCl, 1% [vol/vol] Nonidet-P40, 10 mM EDTA). Extracts were used for immunoblot. Nitrocellulose membranes were stained with Ponceau S for similar protein loading control. The following antibodies were used: RNH1 (catalog H00006050-D01P, Abnova), mouse GATA1 (catalog Sc-265, Santa Cruz Biotechnology Inc.), RPS3 (catalog sc-135390, Santa Cruz Biotechnology Inc.), RPL11 (catalog sc-25931, Santa Cruz Biotechnology Inc.), human RNH1 (catalog sc-365783, Santa Cruz Biotechnology Inc.), human FOG (catalog sc-376189. Santa Cruz Biotechnology Inc.), human GATA1 (catalog 4591, Cell Signaling Technology), BCR (catalog 3902, Cell Signaling Technology) and RPS6 (catalog 2317, Cell Signaling Technology), human C/EBPα, (catalog 2295, Cell Signaling Technology), anti-human PU.1 (catalog 2258, Cell Signaling Technology), EEF2 (catalog 2332, Cell Signaling Technology), β-actin (catalog ab8227, Abcam), and human EKLF/KLF1 (catalog ab2483, Abcam).

Histology. Embryos were embedded in paraffin, and sections were used for H&E staining with routine protocols. Similar sections were used for benzidine staining. Cytospins were prepared from yolk sac cells and stained with Pappenheim stain (May-Grünwald and Giemsa, Fluka).

CRISPR/CAS9-mediated knockout cell line generation. CRISPR sequences targeting exon 2 (RNH1-KO-1) and exon 3 (RNH1-KO-2) of human RNH1 were designed using the online-available CRISPR design tool developed by the F. Zhang laboratory (http://crispr.mit.edu/). The seed sequences preceding the protospacer adjacent motif (PAM) were the following: RNH1-1 oligo 1, 5′-*CAC*-*C*GCGGCGTGCATTGCGTGCTCC-3′; RNH1-1oligo 2, 5′-*AAAC*-GGAGCACGCAATGCACGCCG*C*-3′; RNH1-2 oligo 1, 5′-*CAC*-*C*GGGGTGCGTAGTGTGCTGGAC-3′; and RNH1-2 oligo 2, 5′-*AAAC*GTCCAGCACACTACGCACCC*C*-3′. Nucleotides in italics show the overhangs necessary for incorporation into the restriction enzymatic site BbsI of LentiCRISPR-v2 vector expressing Cas9 and sgRNA (Adgene, catalog 52961) (41). Lentiviruses were produced in 293T cells as previously described (42). K562 cells were infected with lentiCRISPv2 viruses targeting RNH1-1, RNH1-2, or control. Positive cells were selected with 2 μg/ml puromycin. RNH1 expression was assessed by Western blot. To obtain full KO cell lines, populations were cloned by limiting dilution and tested again by Western blot. All the generated K562 clones tested negative for mycoplasma contamination using the MycoAlert Mycoplasma Detection Kit (Lonza, catalog LT07-318). K562 cells were from ATCC, and the presence of the BCR/ABL fusion gene was authenticated by Western blot (Figure 7A) and cytogenetics (data not shown).

RNA-seq and analysis. Total RNA from control K562 and *RNH1*-KO cells was isolated and purified with QIAGEN RNeasy Kit according to the manufacturer's protocol. We prepared Illumina TruSeq stranded mRNA libraries. The libraries were subjected to a preparative size selection on a PippinHT instrument to exclude library molecules with insert sizes of less than 300 bp. Libraries were then sequenced with 2 × 150 bp reads on an Illumina HiSeq3000 instrument.

RNA-seq reads were mapped to the human reference genome (GRCh38, build 81) using Tophat v. 2.0.11 (43). We then used HTseq-count v. 0.6.1 (44) to count the number of reads per gene and DESeq2 v.1.4.5 (45) to test for differential expression between groups of samples. The outcome of the DESeq2 analysis was taken to perform GSEA using the SetRank method (46). This algorithm principally discards gene sets that have initially been flagged as significant, if their significance is merely due to the overlap with another gene set. This method then calculates the P value of a gene set utilizing the ranking of its genes in the ordered list of P values as determined by DESeq2. We constructed a gene set database that consisted of the target gene sets of the GATA1 TF. Next, this database was complemented with all pathways that significantly intersect (Fisher's exact test, Holm-corrected $P \leq 0.01$) with GATA1 target gene sets. The pathway collections searched came from the following databases: BIOCYC (47), Gene Ontology

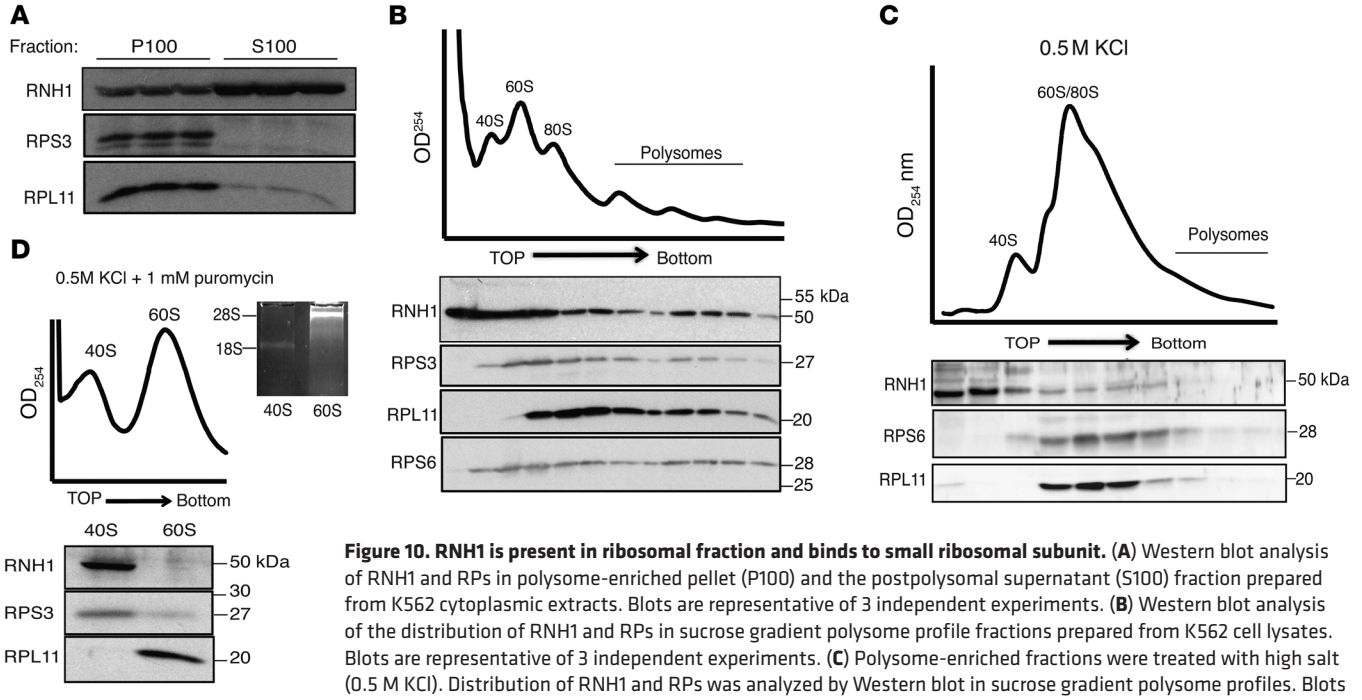

Figure 10. RNH1 is present in ribosomal fraction and binds to small ribosomal subunit. (**A**) Western blot analysis of RNH1 and RPs in polysome-enriched pellet (P100) and the postpolysomal supernatant (S100) fraction prepared from K562 cytoplasmic extracts. Blots are representative of 3 independent experiments. (**B**) Western blot analysis of the distribution of RNH1 and RPs in sucrose gradient polysome profile fractions prepared from K562 cell lysates. Blots are representative of 3 independent experiments. (**C**) Polysome-enriched fractions were treated with high salt (0.5 M KCl). Distribution of RNH1 and RPs was analyzed by Western blot in sucrose gradient polysome profiles. Blots are representative of 3 independent experiments. (**D**) Polysome-enriched fractions were dissociated to 40S and 60S ribosomal subunits with puromycin. The distribution of RNH1 and RPs in pooled fractions was analyzed by Western blot in sucrose gradient polysome profiles. Blots are representative of 3 independent experiments. 18S and 28S rRNA from pooled 40S and 60S fractions were analyzed to check the purity of the 40S and 60S subunits, respectively.

(48), KEGG (49), Pathway Interaction Database (50), REACTOME (51), and WikiPathways (52). The purpose of adding these additional gene sets was to make sure that the observed significance of the GATA1 target gene set was not purely due to this set intersecting with a more significant pathway.

Ribosome profile analysis by sucrose gradient density ultracentrifugation. Yolk sac cells derived from *Rnh1*$^{+/-}$ and *Rnh1*$^{-/-}$ were pooled and cultured for 7 days in methylcellulose semi-solid medium containing all essential growth factors that support erythroid progenitors (M3436, Stem Cell Technologies) to get enough cells. Approximately 2×10^6 yolk sac–derived cells and 5×10^6 K562 cells were washed with PBS containing cycloheximide (CHX) (100 ug/ml) and resuspended in 200 μl of hypotonic buffer (1.5 mM KCl, 2.5 mM $MgCl_2$, and 5.0 mM Tris-Cl, pH 7.4) and 200 μl hypotonic lysis buffer (same with 2% sodium deoxycholate, 2% Triton X-100, and 2.5 mM DTT) plus CHX and gently disrupted using a Dounce homogenizer. The lysates were centrifuged at 8,000 *g* for 10 minutes at 4°C. The supernatant was supplemented with 80 μl heparin. Linear 10% to 45% sucrose gradients (80 mM NaCl, 5 mM $MgCl_2$, 20 mM Tris-Cl, pH 7.4, and 1 mM DTT) were formed manually. Gradients were centrifuged at 230,000 *g* for 3 hours at 4°C and separated through a live OD 254 nm ultraviolet spectrometer. All experiments were repeated at least 3 times under the same conditions.

Protein samples from all fractions were isolated and Western blot was performed for RPS3 or RPS6 and RPL11 present in the 40S and 60S subunits, respectively. Monosomes, both light and heavy polysome fractions, were determined as reported previously (53). TRIzol Reagent (Invitrogen) was added to each collected fraction, and RNA was isolated according to the manufacturer's protocol. Reverse transcription and RT-PCR were performed as mentioned previously. 18S rRNA primers were used for normalization of abundance of the mRNA of interest in monosome and polysome gradient fractions. Gene-specific primers (Microsynth) were used as listed in Supplemental Table 6.

Fractionation of ribosome. Polysome-enriched pellet (P100) and a postpolysomal supernatant (S100) were prepared from cytoplasmic extracts as reported previously (32). To completely dissociate 40S and 60S ribosomal subunits, polysome-enriched pellets were resuspended in a buffer containing 3 mM $MgCl_2$ and 500 mM KCl, and puromycin was added to a final concentration of 1 mM as reported previously (32). Samples were incubated at 37°C for 15 minutes and centrifuged twice for 15 minutes at 30,000 *g*, and the supernatant was loaded on a linear sucrose gradient (10%–30%) in the same buffer. The gradient fractions were collected as described above. Following fractionation, proteins were isolated by precipitating with methanol and chloroform method and Western blotted as described above with anti-RPL11, anti-RPS3 (Santa Cruz Biotechnology Inc.), anti-RPS6 (Cell Signaling), and anti-RNH1 (Abnova).

Generation of RNH1 expression plasmids. The sequence encoding human full-length RNH1 was amplified by PCR and subcloned into the mammalian expression vector pCR3 in frame with the N-terminal Flag or VSV tag. Using the Site-Directed Mutagenesis Kit (Agilent technologies), we generated different RNH1 mutant plasmids and checked their binding with RNase1 (54) (see also Supplemental Figure 10A). RNase1 expression plasmid with the C-terminal MYC/Flag tag was purchased from Origene.

Generation of stable K562 cells expressing Flag-RNH1 and RNH1ΔC. Flag-RNH1or RNH1ΔC was further subcloned into retroviral vector pMSCVpuro (Clonetech). Retroviral vector pMSCVpuro-Flag-RNH1 or RNH1ΔC was cotransfected with the helper plasmids VSV-G and Hit60 into HEK293T cells using PEI transfection reagent. Culture supernatants containing recombinant viral particles were harvested

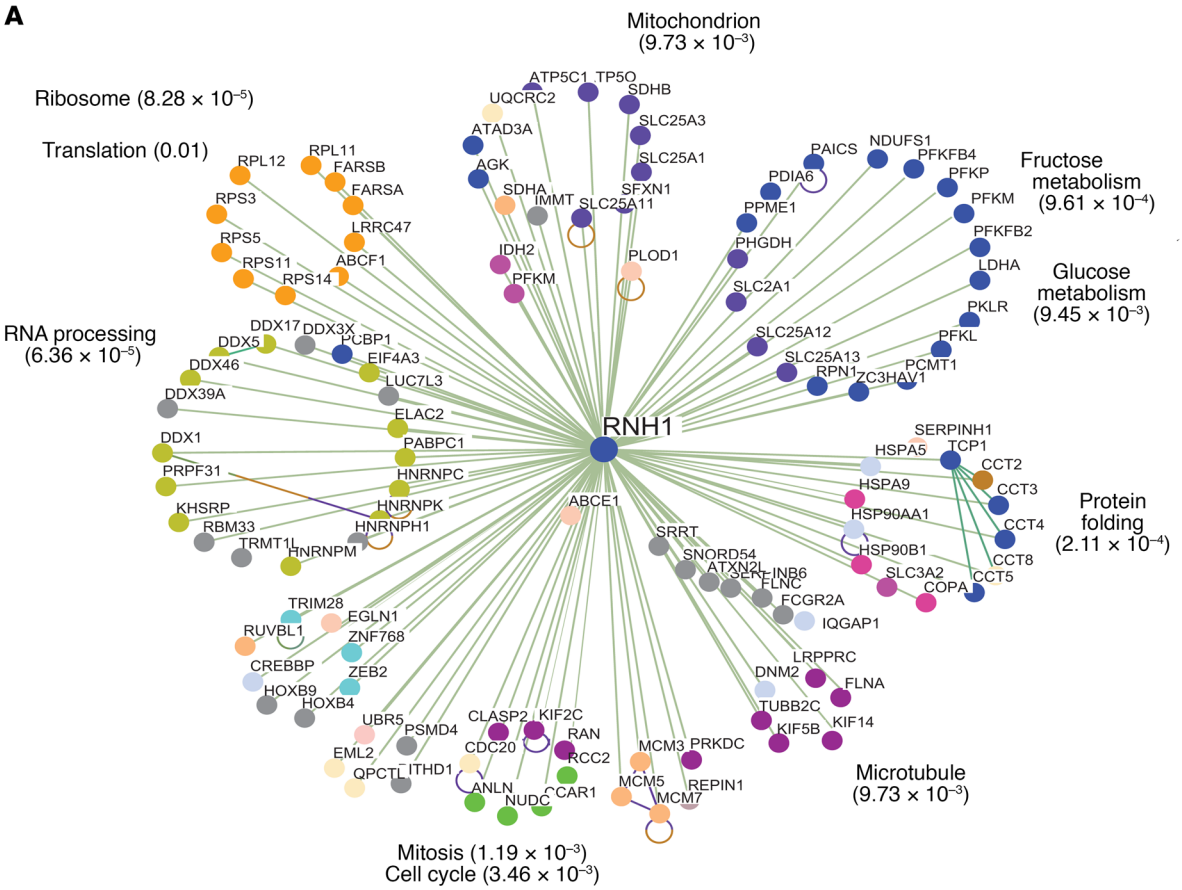

Figure 11. RNH1 binds to RPs. (**A**) Functional enrichment analysis of RNH1-binding proteins identified by MS (Benjamini-Hochberg adjusted *P* values < 0.05). Protein interaction networks were visualized using Osprey. (**B**) Whole cell lysates of stable K562 cells expressing mock or Flag-RNH1 vectors (left) were used for anti-Flag immunoprecipitation and immunoblotting, as indicated (right). Blots are representative of 3 independent experiments.

and used to infect K562 cells. To establish stable cell lines, K562 cells were selected with puromycin (5 μg ml^{-1}) 3 days after infection.

GATA1 rescue experiments. GATA1 expression plasmid was generated as described previously (6). The empty HMD and HMD-GATA1 vectors were transfected with lipofectamine (Invitrogen) in *RNH1*-KO K562 cells and infected with lentivirus vectors in E9.5 *Rnh1*-deficient mouse yolk sac cells. At 48 hours after transfection or after infection, transfection or transduction efficiency was monitored by GFP expression (both vectors contain GFP). GFP-positive cells were enriched by FACS sorting and used to perform benzidine staining and Western blot with K562 cells. In the case of yolk sac cells, GFP-positive cells were cultured for 7 days in methyl cellulose medium, which supports erythroid differentiation.

Immunoprecipitation and MS analyses. Stable mock construct– and Flag-RNH1–expressing K562 cells were resuspended in lysis buffer (20 mM Tris, pH 7.4, 150 mM NaCl, 1% [vol/vol] Nonidet-P40, 10 mM EDTA). In other experiments, Flag- or VSV-tagged constructs and empty vector, as shown in Supplemental Figure 10A, were transfected into HEK293T cells by the calcium-phosphate method. At 24 hours after transfection, cells were resuspended in lysis buffer as mentioned above. Extracts were immunoprecipitated with anti-Flag or anti-VSV agarose beads and then were assessed by immunoblot. For MS analyses, beads after immunoprecipitation were washed with PBS and resuspended in 1× SDS gel-loading buffer to extract bound proteins. Samples were resolved on a 10% mini-polyacrylamide gel for about 2 cm, fixed, and rapidly stained with Coomassie blue. Entire gel lanes

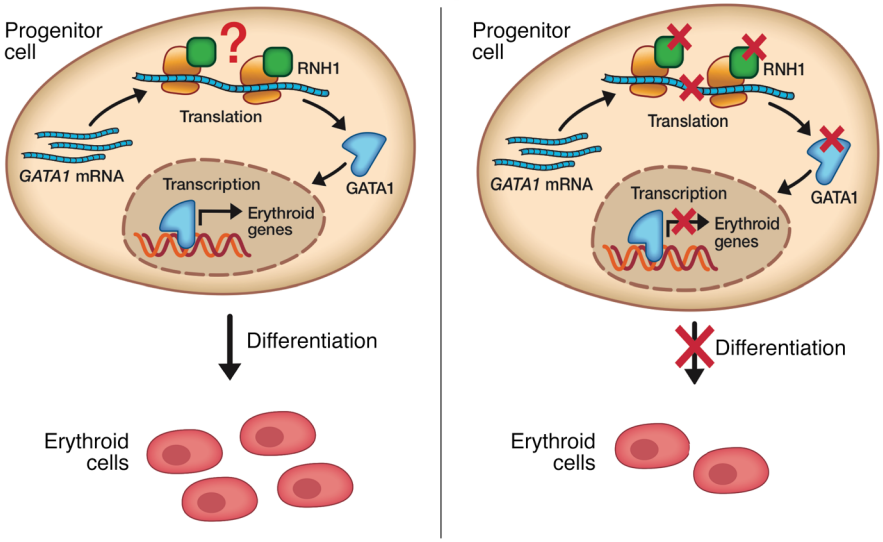

Figure 12. RNH1 is a ribosomal-associated protein that regulates erythropoiesis by controlling GATA1 translation. RNH1 is a ribosomal-associated protein involved in translation of GATA1, which leads to efficient differentiation of progenitor cells to mature erythroid cells. Lack of RNH1 decreases GATA1 levels, which leads to an arrest in differentiation.

were excised into 5 equal regions from top to bottom and digested with sequencing-grade trypsin (Promega) as described (55). Data-dependent liquid chromatography–tandem MS (LC-MS/MS) analysis of extracted peptide mixtures after digestion was carried out on a hybrid linear trap LTQ-Orbitrap Velos mass spectrometer (Thermo Fisher Scientific) interfaced via a nanoelectrospray source to a Dionex 3000 RSLC nanoflow UHPLC. Peptides were separated on a Dionex Pepmap C18 (75 μm ID × 250 mm, 2 μm) capillary column (Dionex) along a 90-minute gradient from 5% to 85% acetonitrile in 0.1% formic acid at a flow rate of 200 nl/minutes. Raw data were used to query a nonredundant protein database using MASCOT software (Matrix Science; version 2.4). Functional enrichment analysis was conducted using DAVID bioinformatics tools (http://david.abcc.ncifcrf.gov/) (56, 57). Protein interaction networks were visualized using Osprey (58). For immune blot, the following antibodies were used: RNH1 (catalog H00006050-D01P, Abnova), RPS3 (catalog sc-135390, Santa Cruz Biotechnology Inc.), RPL11 (catalog sc-25931, Santa Cruz Biotechnology Inc.), RPS6 (catalog 2317, Cell Signaling Technology), EEF2 (catalog 2332, Cell Signaling Technology), β-actin (catalog ab8227, Abcam), and Flag-Ab (catalog F1804 Sigma-Aldrich).

Protein labeling and immunoprecipitation coupled to Click-iT reaction. Click-iT reaction was performed as described previously (6). Briefly, WT and RNH1-KO K562 cells were washed with warm PBS and incubated in methionine-free RPMI medium (R7513, Sigma-Aldrich) with 10% FBS and 2 mM L-glutamine for 1 hour at 37°C, 5% CO_2, to deplete methionine reserves. For labeling, Click-iT AHA (l-azidohomoalanine, C10102, Life Technologies) was added at a final concentration of 50 μM for 4 hours at 37°C, 5% CO_2. Cells were washed twice in cold PBS and resuspended in lysis buffer (20 mM Tris, pH 7.4, 150 mM NaCl, 1% [vol/vol] Nonidet-P40, 10 mM EDTA) supplemented with protease inhibitor cocktail (S8820, Sigma-Aldrich). Cell lysates were prepared by incubation for 30 minutes on ice and centrifugation at 16,000 *g* for 10 minutes at 4°C to remove cellular debris. Using these whole cell lysates, immunoprecipitation was performed with GATA1 antibody (catalog 4591, Cell Signaling Technology) bound to Dynabeads Protein G (10003D, Life Technologies) for 3 hours with rotation at 4°C. The antibody-antigen complex was washed 3 times with lysis buffer, and the Click-iT reaction was performed using TAMRA alkyne and the Click-iT Protein Reaction Buffer Kit (C10276, Invitrogen) for 1 hour at 4°C according to the manufacturer's instructions. The immunoprecipitate was washed once with lysis buffer; then bound proteins were eluted in SDS sample buffer (3×) by heating at 70°C for 10 minutes. Western blot was performed using antibodies against GATA1 or TAMRA (MA1-041, Invitrogen)

Lentiviral production. Lentiviral shRNA plasmids against RNH1 were purchased from MilliporeSigma. Lentiviruses for shRNA were produced by cotransfecting HEK293T cells with the shRNA-containing plasmid targeting RNH1 or scramble (pLKO.1 plasmids: shRNH1, 5′-CCGGGCTGGTCCTGTACGACATTTACTCGAGTAAATGTCGTACAGGACCAGCTTTTTG-3′;5′;shScramble,5′-CCGGCAACAAGATGAAGAGCACCAACTCGAGTTGGTGCTCTTCATCTTGTTGTTTTT-3′) plus a lentiviral packaging system (pMD2 VSV and pCMV DR8.91). Cells were transfected using Lipofectamine 2000 transfection reagent (Invitrogen). Supernatant was collected at 72 hours after transfection and filtered with a 0.45 mm filter to clear cell debris. 30 ml of virus containing supernatant was collected and passed through a Whatman Puradisc 45 μm filter (GE Healthcare Life Sciences, catalog 6780-2504). After addition of 7.5 ml PBS, 1.3 ml of 5 M NaCl, and 8 ml PEG 8000 solution, the mixture was incubated at 4°C on a rotation wheel overnight. PEG 8000 solution was prepared by dissolving 200 g polyethylene glycol 8000 (Carl Roth, catalog 0263) in 200 ml of PBS, followed by autoclave treatment. The virus was precipitated the next day by centrifugation at 3,220 *g* at 4°C for 1 hour. The virus-containing pellet was resuspended in PBS and stored at –80°C until use.

Isolation of primary human CD34⁺ HSPCs. Primary human CD34⁺ HSPCs were isolated from G-CSF–mobilized peripheral blood using the CD34 MicroBead Kit (Miltenyi Biotec, catalog 130-046-702) according to the manufacturer's protocol. Purity was assessed by flow cytometry using a PE-conjugated anti-human CD34 antibody (Miltenyi Biotec, catalog 130-098-140) and was at least 94%.

Expansion and lentiviral infection of primary human CD34⁺ HSPCs. After isolation, primary human CD34⁺ HSPCs were expanded in StemSpan SFEM (Stemcell Technologies, catalog 09600) supplemented with StemSpan CC100 (Stemcell Technologies, catalog 02690) for 5 days (expansion phase). Lentiviral infection was started on day 2 of the expansion phase and continued for a total of 12 hours. For this purpose, cells were cultured at a density of 10^6 cells/ml. Con-

centrated virus was added at a ratio of 1:20 and polybrene (Santa Cruz Biotechnology Inc., catalog sc-134220) at a concentration of 8 μg/ml. Selection was carried out for 30 hours after washing by the addition of 1 μg/ml puromycin (Sigma-Aldrich, catalog P9620). After the expansion phase, cells were counted and split into 2 portions. One portion was used for in vitro erythroid differentiation and the other one for in vitro neutrophilic differentiation.

In vitro erythroid differentiation. In vitro erythroid differentiation was adapted from a previously published protocol (59). In phase 1 (days 0–6), cells were cultured at a density of 10^5–10^6 cells/ml in IMDM (Gibco, Thermo Fisher Scientific; catalog 21980-032) supplemented with 3% human AB serum and 2% human AB plasma (Interregional Blood Transfusion SRC), 1% penicillin/streptomycin (Gibco, Thermo Fisher Scientific; 15070-063), 3 IU/ml heparin (Sigma-Aldrich, catalog H3149), 200 μg/ml holo-transferrin (Sigma-Aldrich, catalog T0665), 10 μg/ml insulin (Sigma-Aldrich, catalog I3536), 1 IU/ml erythropoietin (PeproTech, catalog 100-64), 10 ng/ml stem cell factor (PeproTech, catalog 300-07), and 1 ng/ml IL-3 (PeproTech, catalog 200-03). In phase 2 (day 6–12), IL-3 was omitted.

In vitro neutrophilic differentiation. In vitro neutrophilic differentiation was adapted from a previously published protocol (60). In phase 1 (days 0–3), cells were cultured at a density of 10^5–10^6 cells/ml in IMDM (Gibco, Thermo Fisher Scientific; catalog 21980-032) supplemented with 10% FCS (Amimed, catalog 2-01F10-I), 1% penicillin/streptomycin (Gibco, Thermo Fisher Scientific; 15070-063), 100 ng/ml stem cell factor (PeproTech, catalog 300-07), and 100 ng/ml IL-3 (PeproTech, catalog 200-03). In phase 2 (days 3–12), G-CSF (PeproTech, catalog 300-23) was also supplemented.

May-Grünwald-Giemsa staining. Cells (50,000) were resuspended in 200 μl culture medium and spun onto a slide in a Cytospin 4 Cytocentrifuge (Thermo Scientific, catalog A78300003) at 40 *g* for 10 minutes. Slides were air-dried for at least 10 minutes. Slides were then stained in May-Grünwald solution (Merck, catalog 1.01424.2500) for 4 minutes, rinsed in deionized water for 2 minutes, stained in Giemsa solution (Merck, catalog 1.09204.0500) for 14 minutes, and rinsed twice in deionized water for 2 minutes and 1 minute, respectively. Photographs were taken with a PMW-10MD camera from Sony using a Carl Zeiss, Axioskop 50 microscope

Statistics. Data are expressed as mean ± SEM or mean ± SD of at least 3 biological replicates. Comparison between 2 groups was performed by 2-tailed *t* test. A value of $P < 0.05$ was considered to be statistically significant. All statistical analyses were calculated using GraphPad Prism. No statistical methods were used to predetermine sample size. The experiments were not randomized, and the investigators were not blinded to allocation during experiments and outcome assessment. Gene expression studies were performed using 3 independent biological replicates from each genotype ($Rnh1^{+/+}$, $Rnh1^{+/-}$, and $Rnh1^{-/-}$). RNA-seq experiments were also performed in triplicate. MS studies were performed once.

Study approval. All animal experiments were approved by the Swiss Federal Veterinary Office (Bern, Switzerland) under valid authorization (BE39/16). Mice were handled according to Swiss Federal Veterinary Office guidelines under valid authorization. Approval for the use of human $CD34^+$ cells was obtained from the Kantonale Ethikkommission (Bern, Switzerland).

Data availability. All data sets generated and analyzed during the current study are available in Supplemental Tables 1–5. Microarray and RNA-seq data that support the findings of the study were deposited in the NCBI's gene expression omnibus (GEO GSE48146). RNA-seq data are available in the ArrayExpress database (www.ebi.ac.uk/arrayexpress, E-MTAB-5162).

Author contributions

RA designed experiments, performed most experimental work, analyzed data, and wrote the manuscript. VC, KMM, and NA helped with experimental work and writing the manuscript. DFTV performed microarray-related analyses and helped with writing the manuscript. AT maintained mouse lines and helped with experimental work. ECWY and MS helped with experimental work. CS and MQ generated and analyzed the RNA-seq and MS data, respectively. MAD, HRM, IR, NF, VGS, and AAS provided reagents and critical suggestions. TH and PS helped with the experimental design, analyzing the data, and writing of the manuscript.

Acknowledgments

We thank Florence Morgenthaler for microscopy (Cellular Imaging Facility, University of Lausanne); Janine Horlbeck and Jean-Christophe Stehle for histopathology (mouse pathology facility, University of Lausanne); Keith Harshman for microarray studies (Center for Integrative Genomics, University of Lausanne). We thank the Next Generation Sequencing (NGS) Platform for RNA-seq studies (University of Bern). This work was supported by the Swiss National Science Foundation (PP00P3_157486 to RA), the Louis Jeantet Foundation, and the Institute for Arthritis Research. We dedicate this work to the memory of Jürg Tschopp who initiated this project and inspired many of us.

Address correspondence to: Ramanjaneyulu Allam, Department of Hematology, Inselspital, Bern University Hospital, University of Bern, Murtenstrasse 40, CH-3008 Bern, Switzerland. Phone: 41.31.632.7753; Email: allam.ramanjaneyulu@dbmr.unibe.ch.

DFTV's present address is: The Jackson Laboratory for Genomic Medicine, Farmington, Connecticut, USA.

KMM's present address is: Institute of Immunology and Immunotherapy and Institute of Metabolism and Systems Research, College of Medical and Dental Sciences, University of Birmingham, Birmingham, United Kingdom.

1. Shi Z, Barna M. Translating the genome in time and space: specialized ribosomes, RNA regulons, and RNA-binding proteins. *Annu Rev Cell Dev Biol*. 2015;31:31–54.
2. Xue S, Barna M. Specialized ribosomes: a new frontier in gene regulation and organismal biology. *Nat Rev Mol Cell Biol*. 2012;13(6):355–369.
3. Kondrashov N, et al. Ribosome-mediated specificity in Hox mRNA translation and vertebrate tissue patterning. *Cell*. 2011;145(3):383–397.
4. Narla A, Hurst SN, Ebert BL. Ribosome defects in disorders of erythropoiesis. *Int J Hematol*. 2011;93(2):144–149.
5. Horos R, et al. Ribosomal deficiencies in Diamond-Blackfan anemia impair translation of transcripts essential for differentiation of murine and human erythroblasts. *Blood*. 2012;119(1):262–272.

6. Ludwig LS, et al. Altered translation of GATA1 in Diamond-Blackfan anemia. *Nat Med*. 2014;20(7):748–753.
7. Dickson KA, Haigis MC, Raines RT. Ribonuclease inhibitor: structure and function. *Prog Nucleic Acid Res Mol Biol*. 2005;80:349–374.
8. Furia A et al. The ribonuclease/angiogenin inhibitor is also present in mitochondria and nuclei. *FEBS Lett*. 2011;585(4):613–617.
9. Kobe B, Deisenhofer J. A structural basis of the interactions between leucine-rich repeats and protein ligands. *Nature*. 1995;374(6518):183–186.
10. Haigis MC, Haag ES, Raines RT. Evolution of ribonuclease inhibitor by exon duplication. *Mol Biol Evol*. 2002;19(6):959–963.
11. Dickson KA, et al. Ribonuclease inhibitor regulates neovascularization by human angiogenin. *Biochemistry*. 2009;48(18):3804–3806.
12. Monti DM, Montesano Gesualdi N, Matousek J, Esposito F, D'Alessio G. The cytosolic ribonuclease inhibitor contributes to intracellular redox homeostasis. *FEBS Lett*. 2007;581(5):930–934.
13. Monti DM, D'Alessio G. Cytosolic RNase inhibitor only affects RNases with intrinsic cytotoxicity. *J Biol Chem*. 2004;279(38):39195–39198.
14. Godin I, Cumano A. The hare and the tortoise: an embryonic haematopoietic race. *Nat Rev Immunol*. 2002;2(8):593–604.
15. Huber TL, Kouskoff V, Fehling HJ, Palis J, Keller G. Haemangioblast commitment is initiated in the primitive streak of the mouse embryo. *Nature*. 2004;432(7017):625–630.
16. McGrath K, Palis J. Chapter 1 Ontogeny of Erythropoiesis in the Mammalian Embryo. In: *Red Cell Development*. Amsterdam, Netherlands: Elsevier; 2008:1–22.
17. Baron MH, Isern J, Fraser ST. The embryonic origins of erythropoiesis in mammals. *Blood*. 2012;119(21):4828–4837.
18. Fujiwara Y, Chang AN, Williams AM, Orkin SH. Functional overlap of GATA-1 and GATA-2 in primitive hematopoietic development. *Blood*. 2004;103(2):583–585.
19. Fujiwara Y, Browne CP, Cunniff K, Goff SC, Orkin SH. Arrested development of embryonic red cell precursors in mouse embryos lacking transcription factor GATA-1. *Proc Natl Acad Sci U S A*. 1996;93(22):12355–12358.
20. Shivdasani RA, Mayer EL, Orkin SH. Absence of blood formation in mice lacking the T-cell leukaemia oncoprotein tal-1/SCL. *Nature*. 1995;373(6513):432–434.
21. Moenner M, Vosoghi M, Ryazantsev S, Glitz DG. Ribonuclease inhibitor protein of human erythrocytes: characterization, loss of activity in response to oxidative stress, and association with Heinz bodies. *Blood Cells Mol Dis*. 1998;24(2):149–164.
22. Ferkowicz MJ, et al. CD41 expression defines the onset of primitive and definitive hematopoiesis in the murine embryo. *Development*. 2003;130(18):4393–4403.
23. Bertrand JY, et al. Characterization of purified intraembryonic hematopoietic stem cells as a tool to define their site of origin. *Proc Natl Acad Sci U S A*. 2005;102(1):134–139.
24. Lancrin C, Sroczynska P, Stephenson C, Allen T, Kouskoff V, Lacaud G. The haemangioblast generates haematopoietic cells through a haemogenic endothelium stage. *Nature*. 2009;457(7231):892–895.
25. Socolovsky M, Nam H, Fleming MD, Haase VH, Brugnara C, Lodish HF. Ineffective erythropoiesis in Stat5a(-/-)5b(-/-) mice due to decreased survival of early erythroblasts. *Blood*. 2001;98(12):3261–3273.
26. Pevny L, et al. Erythroid differentiation in chimaeric mice blocked by a targeted mutation in the gene for transcription factor GATA-1. *Nature*. 1991;349(6306):257–260.
27. Sankaran VG, et al. Exome sequencing identifies GATA1 mutations resulting in Diamond-Blackfan anemia. *J Clin Invest*. 2012;122(7):2439–2443.
28. Koeffler HP, Golde DW. Human myeloid leukemia cell lines: a review. *Blood*. 1980;56(3):344–350.
29. O'Brien KA, et al. Molecular convergence in ex vivo models of Diamond-Blackfan anemia. *Blood*. 2017;129(23):3111–3120.
30. Crossley M, Tsang AP, Bieker JJ, Orkin SH. Regulation of the erythroid Kruppel-like factor (EKLF) gene promoter by the erythroid transcription factor GATA-1. *J Biol Chem*. 1994;269(22):15440–15444.
31. Welch JJ, et al. Global regulation of erythroid gene expression by transcription factor GATA-1. *Blood*. 2004;104(10):3136–3147.
32. Dresios J, Aschrafi A, Owens GC, Vanderklish PW, Edelman GM, Mauro VP. Cold stress-induced protein Rbm3 binds 60S ribosomal subunits, alters microRNA levels, and enhances global protein synthesis. *Proc Natl Acad Sci U S A*. 2005;102(6):1865–1870.
33. Reschke M, et al. Characterization and analysis of the composition and dynamics of the mammalian riboproteome. *Cell Rep*. 2013;4(6):1276–1287.
34. Narla A, Ebert BL. Ribosomopathies: human disorders of ribosome dysfunction. *Blood*. 2010;115(16):3196–3205.
35. Haigis MC, Kurten EL, Raines RT. Ribonuclease inhibitor as an intracellular sentry. *Nucleic Acids Res*. 2003;31(3):1024–1032.
36. Allam R, Lichtnekert J, Moll AG, Taubitz A, Vielhauer V, Anders HJ. Viral RNA and DNA trigger common antiviral responses in mesangial cells. *J Am Soc Nephrol*. 2009;20(9):1986–1996.
37. Gautier L, Cope L, Bolstad BM, Irizarry RA. affy--analysis of Affymetrix GeneChip data at the probe level. *Bioinformatics*. 2004;20(3):307–315.
38. Breitling R, Armengaud P, Amtmann A, Herzyk P. Rank products: a simple, yet powerful, new method to detect differentially regulated genes in replicated microarray experiments. *FEBS Lett*. 2004;573(1-3):83–92.
39. Hannah R, Joshi A, Wilson NK, Kinston S, Göttgens B. A compendium of genome-wide hematopoietic transcription factor maps supports the identification of gene regulatory control mechanisms. *Exp Hematol*. 2011;39(5):531–541.
40. Subramanian A, et al. Gene set enrichment analysis: a knowledge-based approach for interpreting genome-wide expression profiles. *Proc Natl Acad Sci U S A*. 2005;102(43):15545–15550.
41. Sanjana NE, Shalem O, Zhang F. Improved vectors and genome-wide libraries for CRISPR screening. *Nat*. 2014;11(8):783–784.
42. Bagnis C, Bailly P, Chapel-Fernandes S. Using an EGFPmeter to Evaluate the Lentiviral Vector Production: Tricks and Traps. In: *Viral Applications of Green Fluorescent Protein*. Totowa, NJ: Humana Press; 2009:151–163.
43. Kim D et al. TopHat2: accurate alignment of transcriptomes in the presence of insertions, deletions and gene fusions. *Genome Biol*. 2013;14(4):R36.
44. Anders S, Pyl PT, Huber W. HTSeq--a Python framework to work with high-throughput sequencing data. *Bioinformatics*. 2015;31(2):166–169.
45. Love MI, Huber W, Anders S. Moderated estimation of fold change and dispersion for RNA-seq data with DESeq2. *Genome Biol*. 2014;15(12):31.
46. Simillion C, Liechti R, Lischer HE, Ioannidis V, Bruggmann R. Avoiding the pitfalls of gene set enrichment analysis with SetRank. *BMC Bioinformatics*. 2017;18(1):151.
47. Karp PD et al. Expansion of the BioCyc collection of pathway/genome databases to 160 genomes. *Nucleic Acids Res*. 2005;33(19):6083–6089.
48. Ashburner M, et al. Gene ontology: tool for the unification of biology. The Gene Ontology Consortium. *Nat Genet*. 2000;25(1):25–29.
49. Kanehisa M, Goto S, Sato Y, Kawashima M, Furumichi M, Tanabe M. Data, information, knowledge and principle: back to metabolism in KEGG. *Nucleic Acids Res*. 2014;42(Database issue):D199–D205.
50. Schaefer CF, et al. PID: the Pathway Interaction Database. *Nucleic Acids Res*. 2009;37(Database issue):D674–D679.
51. Croft D, et al. The Reactome pathway knowledgebase. *Nucleic Acids Res*. 2014;42(Database issue):D472–D477.
52. Kelder T, et al. WikiPathways: building research communities on biological pathways. *Nucleic Acids Res*. 2012;40(Database issue):D1301–D1307.
53. Park EH, Zhang F, Warringer J, Sunnerhagen P, Hinnebusch AG. Depletion of eIF4G from yeast cells narrows the range of translational efficiencies genome-wide. *BMC Genomics*. 2011;12:68.
54. Lee FS, Vallee BL. Modular mutagenesis of human placental ribonuclease inhibitor, a protein with leucine-rich repeats. *Proc Natl Acad Sci U S A*. 1990;87(5):1879–1883.
55. Wilm M, et al. Femtomole sequencing of proteins from polyacrylamide gels by nano-electrospray mass spectrometry. *Nature*. 1996;379(6564):466–469.
56. Huang da W, Sherman BT, Lempicki RA. Systematic and integrative analysis of large gene lists using DAVID bioinformatics resources. *Nat Protoc*. 2009;4(1):44–57.
57. Huang da W, Sherman BT, Lempicki RA. Bioinformatics enrichment tools: paths toward the comprehensive functional analysis of large gene lists. *Nucleic Acids Res*. 2009;37(1):1–13.
58. Breitkreutz BJ, Stark C, Tyers M. Osprey: a network visualization system. *Genome Biol*. 2003;4(3):R22.
59. Giani FC, et al. Targeted application of human genetic variation can improve red blood cell production from stem cells. *Cell Stem Cell*. 2016;18(1):73–78.
60. Gupta D, Shah HP, Malu K, Berliner N, Gaines P. Differentiation and characterization of myeloid cells. *Curr Protoc Immunol*. 2014;104:Unit 22F.5.